2009

Light front Hamiltonian and its application in QCD

Jun Li
Iowa State University

Light front Hamiltonian and its application in QCD

by

Jun Li

A dissertation submitted to the graduate faculty

in partial fulfillment of the requirements for the degree of

DOCTOR OF PHILOSOPHY

Major: Nuclear Physics

Program of Study Committee:
James Vary, Major Professor
Alexander Roitershtein
Marzia Rosati
Kirill Tuchin
Kerry Whisnant

Iowa State University

Ames, Iowa

2009

DEDICATION

To my family

TABLE OF CONTENTS

LIST OF TABLES

LIST OF FIGURES

ACKNOWLEDGEMENTS

I would like to take this opportunity to express my thanks to my major professor Dr. Vary for his guidance, patience and support throughout this research and the writing of this thesis. Even after I finished this dissertation, I still remember his words of encouragement which has inspired me and renewed my hopes for obtaining this Ph.d degree in physics.

I would also like to thank all the professors in physics department of ISU, who have taught me physics in nearly every area. Specially I want to thank Dr. Luban who taught me EM course, which was the first interesting course I took at ISU. I also appreciate his help on derivation of hypergeometric functions in one of my projects. Many thanks go to Dr. Anderson who gave me opportunity to be a teaching assistant for the general relativity, which forces me to refresh my knowledge on this area to face the challenge from the students in this class.

I also thank my friends Oleg Antipin and previous Postdoctoral Research Associate Piyabut Burikham who taught me that the inspiration of physics can even be produced in the bar. Thanks also go to my research group members Heli Honkanen, Pieter Maris, Alina Negoita for discussion on physics. I would like to thank a collaborator, Dr. Avaroth Harindranath, for his guidance on the derivations in Chapter 2.

From the bottom of my heart, I want to thank my parents, Xiulan Meng and Guoyi Li, not only for having me in the first place, but for believing in me all these years no matter what I have chosen to do.

I would like to express my deep appreciation and love to my wife, Yan Lin, who always stays with me not only to suffer the countless hours of my solitude but also to share the happiness of the life. Without her support, I cannot imagine that I could have completed this work.

Finally, I want to thank my daughter, Sherry Li, for the joy she brings to the whole family.

CHAPTER 1. QUANTUM CHROMODYNAMICS

Quantum Chromodynamics or QCD is a fundamental theory of the strong interaction. It is a non-Abelian gauge theory which has SU(3) symmetry. The quarks have 3 colors whose transformation in color space can be described by SU(3) in the fundamental representation. To have local invariance under the SU(3) transformation, gauge particles (gluons) are introduced into the Lagrangian. The difference between Abelian and non-Abelian gauge theory is whether gauge particles can carry charge. In a non-Abelian gauge theory, such as QCD, gluons carry charge. Therefore gluons can interact with themselves. Gluons have 8 colors whose transformation in color space can be described by SU(3) in the adjoint representation.

At short distance, probed with high momentum transfer experiments, the coupling constant of QCD becomes small and this infers that the theory has a property called asymptotic freedom [1, 2]. Therefore perturbative calculations are allowed for high momentum transfer experimental quantities such as cross sections. Furthermore, it is frequently the case that the cross section can be obtained by using a factorization method [3] by which the cross section can be factorized into a perturbative part and non-perturbative part. In the factorization approach, the perturbative part can be calculated from the Feynman diagrams ordered by coupling constant. The non-perturbative part, for the case of multiparticle production, can be explained as parton distribution functions and fragmentation functions which are universal and can be determined from the experiment. These non-perturbative components are said to be universal since they are determined by a limited number of experiments but apply to a broad class of additional experiments. One of the aims of this thesis is to help pave a pathway to calculating these non-perturbative quantities for comparison with experiment.

On the other hand, the QCD coupling constant becomes larger when the momentum trans-

ferred becomes smaller which leads to the phenomenon called confinement. Confinement dictates that there are no free quarks in nature. What we observe are the bound states of quarks and gluons which are colorless. That is, the colors in the observed bound state systems combine in such a way as to produce no net color in analogy with white light which is constructed from a spectrum of colors. To solve for the bound states in this strong interaction regime of QCD, a suitable non-perturbative method must be found. One of these methods is the Hamiltonian method. By diagonalizing the Hamiltonian matrix in a suitable Fock space basis, the eigenvalues and eigenvectors of bound states of quarks and gluons can be obtained. The eigenstates, which are then expressed as superpositions of Fock space basis states, can then be analyzed to yield the non-perturbative parton distribution functions and fragmentation functions.

A major goal here is to define symmetry-restricted Fock space basis spaces suitable for evaluating the bound states of multiple quarks and gluons in QCD.

1.1 Quarks

The proton and neutron are not fundamental particles. They are understood to be primarily composed of three constituents called quarks in a simple picture that is best illustrated with the following simple analysis. The magnetic dipole moment μ of a pointlike particle, such as the electron, is proportional to the charge q, the total spin S, the constant g, and inversely proportional to the mass m particle:

$$\mu = \mathbf{g}(\frac{\mathbf{q}}{\mathbf{2m}})\mathbf{S}. \tag{1.1}$$

As a result, if the neutron were pointlike it would have zero magnetic moment since it carries no charge. However from experiment, the magnetic moment of the neutron is not zero, which implies it has internal structure. In 1963 Gell-Mann [4] and Zweig [5] independently proposed the quark model, according to which hadrons (mesons and baryons) are composite particles composed of two (mesons) or three (baryons) fundamental particles called quarks. According to QCD, which soon emerged to replace these early quark models, each quark has one of 6 flavors which are u,d,s,c,b and t with charges +2/3, -1/3, -1/3, +2/3, -1/3 and +2/3. By using

the quark model, the magnetic moment of the neutron, which can be treated in its leading Fock space basis state as the three valence quark configuration $|udd\rangle$, can be calculated as the sums of magnetic moments arising from the constituent quarks: $\mu_n = \frac{4}{3}\mu_d - \frac{1}{3}\mu_u$. The magnetic moment of the proton, which has the leading Fock space component $|uud\rangle$, is $\mu_p = \frac{4}{3}\mu_u - \frac{1}{3}\mu_d$. If we assume that the masses of u and d quarks are equal, then $\mu_u = -2\mu_d$ which leads to the ratio between magnetic dipole moments of a neutron and a proton

$$\frac{\mu_n}{\mu_p} = \frac{\frac{4}{3}\mu_d - \frac{1}{3}\mu_u}{\frac{4}{3}\mu_u - \frac{1}{3}\mu_d} = \frac{2\mu_d}{-3\mu_d} = -\frac{2}{3}. \tag{1.2}$$

This result is very close to the experimental result which is -0.685.

In order to retain Fermi-Dirac statistics for the known baryons and mesons when constructing them from quarks, an additional degree of freedom called color is introduced. The total wavefunction of three quarks must be antisymmetric for baryons due to the requirement of Fermi-Dirac statistics. However, the $\triangle^{++}$ as a uuu bound state is symmetric under the interchange of the quark spin and flavor quantum number. With the supplement of an antisymmetric wavefunction in color space, the total wavefunction of the $\triangle^{++}$ is antisymmetric. Furthermore, in order to satisfy confinement, the wavefunction of baryons, mesons and even exotic multiparton hadrons are taken to be singlet states (colorless states) in color space. We will present detailed methods for constructing color singlet states for arbitrary multiparton hadrons in chapter 4.

The quark model is very successful since it explains many properties of the mesons and baryons including the cited example above of the ratio of neutron to proton magnetic moments. It also predicts the existence of new particles such as the Ω^-. However it also has some problems. For example, the quark model alone does not predict confinement. In addition, there is no role for interactions (absence of dynamics) in the quark model. For example, we would like to have interactions that tell us how three quarks are held together to form a proton or a neutron. For the dynamics which can describe the interaction between quarks, Quantum Chromodynamics or QCD is adopted in which non-Abelian gauge bosons (gluons) act between the quarks and among themselves [6, 7].

1.2 Lagrangian of QCD

Quantum Chromodynamics or QCD is the widely accepted fundamental theory of the strong interaction. It describes the interaction between quarks via non-Abelian gauge bosons called gluons which can also interact with themselves. We will proceed now to introduce the Lagrangian of QCD in a sequence of steps.

We begin with the free-particle Lagrangian $\mathcal{L}_f$ for the quarks which are described by fermion fields $\psi(x)$, having spin 1/2

$$\mathcal{L}_f = \bar{\psi}(x)(i\gamma^\mu \partial_\mu - m)\psi(x), \tag{1.3}$$

where quark field $\psi(x) \equiv \psi^f_{i,a}(x)$. "$f$" represents flavor which can be u, d, s, c, b, t. "i" represents spinor with $i = 1, 2, 3, 4$. And "a" represents one of three colors.

In the equation above, γ^μ are Dirac gamma matrices and m represents the mass of quark. To account for the quark's color degree of freedom, $\psi(x)$ has components in color space where its transformation can be described by SU(3) in the fundamental representation:

$$\psi(x) \to V\psi(x), \tag{1.4}$$

where $V = \exp(i\alpha^a t^a)$ and t^a are generators of SU(3) transformation and have the commutation relations in the form

$$[t^a, t^b] = if^{abc}t^c, \tag{1.5}$$

and f^{abc} are the structure constants of the SU(3) transformation and the color indices a, b and c run from 1 to 8. The quantities, α^a, are arbitrary coefficients.

In Eqn. (1.4), if α^a does not depend on x, then it is obvious that Eqn. (1.3) is invariant under the SU(3) transformation since $\bar{\psi}(x) \to \bar{\psi}(x)V^\dagger$ and $V^\dagger V = 1$. However it is not invariant under a local SU(3) gauge transformation where α^a can be a function of x since the derivative would then play a role. In order to retain the SU(3) local gauge invariance, the gauge particles are introduced by replacing ∂ in Eqn. (1.3) with the covariant derivative

$$D_\mu = \partial_\mu - igA^a_\mu t^a, \tag{1.6}$$

where A^a_μ represents the non-Abelian gauge field with color indices a running from 1 to 8. And g is strong coupling constant.

Under the local SU(3) gauge transformation,

$$D_\mu \psi \to V(x) D_\mu \psi, \tag{1.7}$$

then $\bar{\psi}(i\gamma_\mu D_\mu - m)\psi$ is invariant. If the field tensor is defined as

$$[D_\mu, D_\nu] = -igF^a_{\mu\nu} t^a, \tag{1.8}$$

then

$$F^a_{\mu\nu} = \partial_\mu A^a_\nu - \partial_\nu A^a_\mu + g f^{abc} A^b_\mu A^c_\nu. \tag{1.9}$$

Under the SU(3) transformation,

$$F^a_{\mu\nu} t^a \to V(x) F^a_{\mu\nu} t^a V^\dagger(x). \tag{1.10}$$

Then the term $-\frac{1}{2}\mathrm{tr}[(F^a_{\mu\nu}t^a)^2] = -\frac{1}{4}(F^a_{\mu\nu})^2$ is gauge invariant since, with the trace calculation, $V^\dagger(x)V(x) = 1$.

The gauge invariant QCD Lagrangian is

$$\mathcal{L} = -\frac{1}{4} F^a_{\mu\nu} F^{\mu\nu}_a + \sum_{\text{flavor}} \bar{\psi}(i\gamma^\mu D_\mu - m)\psi, \tag{1.11}$$

where we have summed over the 6 flavors and suppressed the indices on the fermion fields and covariant derivatives as they are now understood from the previous definitions.

Some comments about Eqn. (1.11):

(1). Under the gauge transformation, the infinitesimal transformation law for A^a_μ is

$$A^a_\mu \to A^a_\mu + \frac{1}{g}\partial_\mu \alpha^a + f^{abc} A^b_\mu \alpha^c. \tag{1.12}$$

There is no term $m^2 A^a_\mu A^\mu_a$ since it is not gauge invariant under the transformation Eqn. (1.12). Therefore the gluon is massless.

(2). The QCD Lagrangian is rather simple though it might not seem so simple when it is first encountered. The Lagrangian has energy dimension 4 - the units are Energy per unit

space-time volume and space-time volume here is in 4 dimensions. In Eqn. (1.11), ψ has dimension $\frac{3}{2}$ and A^a_μ has dimension 1. We readily see that there can be no higher order gauge invariant terms which contain ψ, A^a_μ and the covariant derivative.

(3). It is a renormalizable theory. The coupling constant g has dimension 0 which satisfies the requirement that a renormalizable theory has coupling constant with dimension no less than 0. This is another reason why there are no higher order gauge invariant terms which contains ψ, A^a_μ and the covariant derivative in the Lagrangian which would lead to coupling constants with dimension less than 0.

(4). Under the infinitesimal gauge transformation

$$F^a_{\mu\nu} \to F^a_{\mu\nu} - f^{abc}\alpha^b F^c_{\mu\nu}. \tag{1.13}$$

From the field strength $F^a_{\mu\nu}$, we can define the Non-Abelian electric and magnetic field:

$$\begin{aligned} E^i_a &= F^{i0}_a, \\ B^i_a &= -\frac{1}{2}\epsilon^{ijk}F^{jk}_a. \end{aligned} \tag{1.14}$$

However unlike QED, the non-Abelian electric field E^i_a and magnetic field B^i_a are not gauge invariant under the gauge transformation Eqn. (1.13). Therefore they are not physically observable quantities.

1.3 Fixing the gauge

There are two methods to quantize the field. One method is canonical quantization where we first obtain the canonical momentum from the Lagrangian. Then using the Poisson bracket, we obtain the commutation relationship between the field and the canonical momentum. One then quantizes the field by expanding it in terms of creation and annihilation operators and applies commutation (Boson) or anti-commutation (Fermion) conditions on these operators. The resulting fields will then obey the commutation or anti-commutation relations as appropriate to their statistics. The other method is the functional integral quantization method: the Green's function or propagator is obtained from the generating function.

However the problem happened in both methods. For example, in functional integral quantization method, $-\frac{1}{4}F^a_{\mu\nu}F^{\mu\nu}_a$ or $\mathcal{L}$ is gauge invariant. Consider the functional integral

$$\int \mathcal{D}A e^{iS[A]},$$
$$S = \int d^4x[-\frac{1}{4}F^a_{\mu\nu}F^{\mu\nu}_a], \tag{1.15}$$

where $\mathcal{D}A$ represents the functional integral over all field configurations. And S is the action for the gauge fields A alone.

Under the gauge transformation Eqn. (1.12), S does not change due to the gauge invariance of $-\frac{1}{4}F^a_{\mu\nu}F^{\mu\nu}_a$. Therefore the functional integral Eqn. (1.15) is divergent due to the integration over a continuous infinity of equivalent field configurations (equivalent under arbitrary gauge transformations). Similarly in canonical quantization method, not all the gauge fields are independent. Therefore, we can not naively obtain the commutation relations between gauge fields and the conjugate momenta.

To remove this divergence, we need to impose a gauge fixing condition such that we consider all equivalent fields once. There are a couple of ways to fix the gauge. A common choice is covariant gauge: $\partial_u A^u = 0$. Under this gauge choice, unphysical particles called ghost particles are required to retain the unitarity of quantum field theory. The argument is given as follows. Since the gluon is massless, it has only two physical transverse polarizations. However from the optical theorem, in Fig. 1.1, the left hand side must be equal to the right hand side. But on the left hand side, the gluon loop has longitudinal polarization. And on the right hand side, the two gluons in final state have only transverse polarizations. In order to retain unitarity, the ghost particle is introduced such that on the left hand side, there is one more diagram with the ghost loop as the intermediate state to remove the longitudinal polarization.

To avoid the ghost particle, the light front gauge can be chosen. Under the light front gauge, $A^+ \equiv A^0 + A^3 = 0$ and from the equation of motion for the gauge field, $A^- \equiv A^0 - A^3$ can be expressed in terms of $A^\perp \equiv (A^1, A^2)$, indicating A^- is no longer independent. Therefore, in light front gauge, gluons only have two transverse polarizations which are independent components. As a result, there is no need for a ghost particle to remove the longitudinal

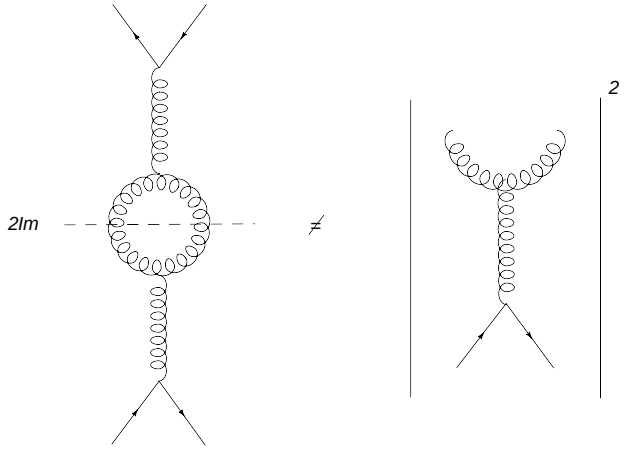

Figure 1.1 From the optical theorem, the left hand side needs to be equal to the right hand side. However with a covariant gauge, the ghost particle is required to remove the unphysical degree of freedom on the left hand side. Therefore the graph on the left hand side is equal to the graph on the right hand side plus one additional graph where the ghost particle is sitting in the middle.

polarizations with the light front gauge. We will adopt the light front gauge for simplicity in what follows.

1.4 Running coupling constant

For a renormalizable theory, the coupling constant is not fixed. To remove the ultraviolet divergence, the renormalization scale is chosen. However the physical quantities should be independent of choice of renormalization scale, which implies that the coupling constant evolutes with external energy in the interaction theory.

In analogy with the fine structure constant, $\alpha \sim 1/137$, in Quantum Electrodynamics (QED), we define coupling constant $\alpha_s = g^2/4\pi$. In QCD, the running coupling constant α_s is determined by the renormalization equation

$$\mu^2 \frac{\partial \alpha_s}{\partial \mu^2} = \beta(\alpha_s). \tag{1.16}$$

$\beta(\alpha_s)$ is calculated and has the perturbative expansion [1, 2, 8, 9]

$$\beta(\alpha_s) = -b_0 \alpha_s^2 (1 + b_1 \alpha_s + b_2 \alpha_s^2 + O(\alpha_s^3)), \tag{1.17}$$

where

$$\begin{aligned} b_0 &= \frac{(33-2n_f)}{12\pi} \\ b_1 &= \frac{(153-19n_f)}{2\pi(33-2n_f)} \\ b_2 &= \frac{(77139-15099n_f+325n_f^2)}{288\pi^2(33-2n_f)}. \end{aligned} \tag{1.18}$$

and n_f is the number of flavors.

If we only consider the leading order in Eqn.(1.17), the Eqn.(1.16) gives us the solution

$$\alpha_s(\mu^2) = \frac{\alpha_s(\mu_0^2)}{1+\alpha_s(\mu_0^2)b_0 t}, \quad t = \ln\frac{\mu^2}{\mu_0^2}, \tag{1.19}$$

where μ is renormalization scale.

Unlike QED, in QCD the coupling constant α_s becomes smaller when μ^2 is larger, which can be shown in Fig. 1.2. This is known as asymptotic freedom.

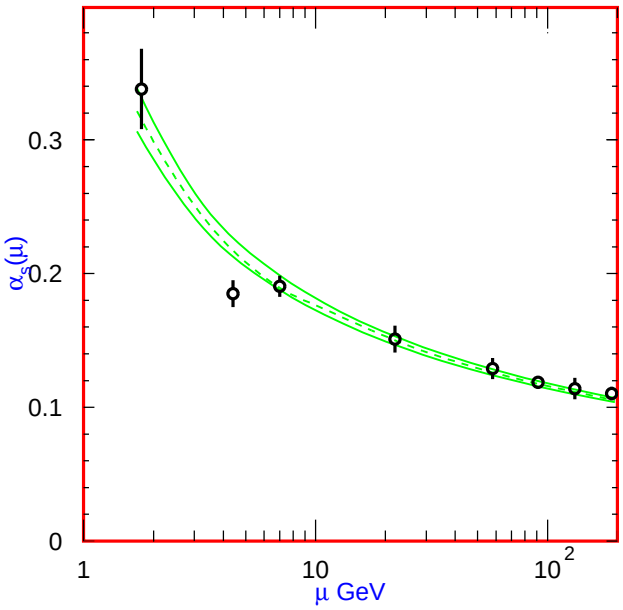

Figure 1.2 The QCD running coupling constant as the function of μ: when μ becomes larger, the running coupling constant becomes smaller.(Figure comes from ref.[10])

Perturbative calculations are allowed when the momentum transferred is sufficiently large. For example, in deep inelastic scattering process, when the virtual photon carries very large

momentum, the cross section can be factorized into a long distance part called parton distribution function and a short distance part which in leading order is the pointlike interaction between the virtual photon and a quark.

On the other hand, when the momentum transferred becomes smaller, the running coupling becomes larger, which leads to the phenomena called confinement. Perturbative calculations fail in this strong coupling regime. In order to solve for experimental quantities such as bound states in this regime, new methods such as the Hamiltonian method we employ here can be used.

CHAPTER 2. LIGHT FRONT QCD HAMILTONIAN

2.1 The general idea of Hamiltonian method

Before we introduce the light front QCD Hamiltonian, we first discuss the general Hamiltonian method. Recall that in non-relativistic quantum mechanics, the Hamiltonian is the sum of kinetic energy and potential energy. We can then solve the Hamiltonian eigenvalue problem to obtain the bound state solutions and their respective eigenfunctions as a Hamiltonian matrix eigenvalue problem in a selected basis space. We will work with the Hamiltonian matrix formulation in this effort. In order to obtain the Hamiltonian, we need to define the canonical momentum from the Lagrangian.

Suppose we have a general Lagrangian $\mathcal{L}$ which is the function of $\phi(x)$ and its derivative $\partial_\mu\phi(x)$. From the Lagrangian $\mathcal{L}$, the canonical momentum is defined as

$$\pi_\phi(x) = \frac{\partial\mathcal{L}}{\partial(\partial_t\phi)}. \tag{2.1}$$

Once we have the canonical momentum $\pi_\phi(x)$, the Hamiltonian is obtained after we integrate over all three-dimensional space,

$$H(x) = \int dx^1dx^2dx^3(\pi_\phi(x)\phi(x) - \mathcal{L}). \tag{2.2}$$

In quantum field theory, the fields are operators. In order to quantize the fields, the equal time canonical commutation relation is given by

$$[\phi(x), \pi_\phi(y)]_{x^0-y^0} = \delta^{(3)}(x-y). \tag{2.3}$$

Here we want to emphasize in Eqn. (2.3), the equal instant time is taken when we quantize the fields. However the equal light front time quantization can also be used when we quantize the fields and this will be our choice once we define the light front variables below.

With canonical commutation relations, the creation operator $a_p^\dagger$ and annihilation operator a_p can be obtained once we expand the field in terms of plane wavefunctions with different four-momenta p,

$$\phi(x) = \int \frac{d^3p}{(2\pi)^3} \frac{1}{\sqrt{2\omega_p}} (a_p e^{ip\cdot x} + a_p^\dagger e^{-ip\cdot x}), \tag{2.4}$$

$$\pi(x) = \int \frac{d^3p}{(2\pi)^3} (-i) \sqrt{\frac{\omega_p}{2}} (a_p e^{ip\cdot x} + a_p^\dagger e^{-ip\cdot x}), \tag{2.5}$$

where $\omega_p = \sqrt{\vec{p}^2 + m^2}$, where $\vec{p}^2$ is the square of the three-momentum.

Then from Eqn. (2.3), we have

$$[a_p, a_q^+] = (2\pi)^3 \delta^{(3)}(p - q). \tag{2.6}$$

Again we want to emphasize in Eqn. (2.6), the equal instant time is taken.

In the case of a Hamiltonian without interaction, the ground state $|0\rangle$ is called the vacuum. When a_p acts on the vacuum, we obtain zero. Therefore, the ground state of the free Hamiltonian is trivial. However, with the interaction, the ground state of the full Hamiltonian $|\Omega\rangle$ is not the same as the ground state of free Hamiltonian $|0\rangle$, in the conventional form of quantum mechanics where the Hamiltonian governs the time evolution of the system from an initial instant in time, t_0. To see the structure of the ground state of the full Hamiltonian $|\Omega\rangle$, we can express it in terms of complete eigenstates of the free Hamiltonian,

$$\langle\Omega| = \langle\Omega|0\rangle\langle 0| + \sum_n \langle\Omega|n\rangle\langle n|, \tag{2.7}$$

where $|n\rangle$ are the multiparticle states. As an example, consider a specific term with 3 pairs in specified momentum states, $|3\rangle$, that can be expressed as

$$|3\rangle = (a_{-p_3} a_{p_3}^+)(a_{-p_2} a_{p_2}^+)(a_{-p_1} a_{p_1}^+)|0\rangle. \tag{2.8}$$

Therefore, even though the total momentum of ground state is zero, it contains an arbitrary number of of virtual particle and antiparticle pairs. Actually, $\langle\Omega|$ is obtained by evolving $|0\rangle$ from time -T to time t_0 with the operator U which is defined as $U(t, t_0) = e^{iH_0(t-t_0)} e^{-iH(t-t_0)}$ [11].

$$\langle\Omega| = \lim_{T\to\infty(1-i\epsilon)} \langle 0|U(T, t_0)(e^{-iE_0(T-t_0)}\langle 0|\Omega\rangle)^{-1}. \tag{2.9}$$

Above we denote H_0 as the free Hamiltonian and H as the full Hamiltonian and E_0 is the ground energy of H.

To avoid this complicated ground state of the full Hamiltonian, the light front form is introduced in the next section where we can see that the structure of the ground state is much simpler.

2.2 Light front form of Hamiltonian

2.2.1 Light front coordinates

The light front form was introduced by Dirac [12]: the initial surface on which the system begins its evolution is the three dimensional surface in space-time formed by a plane wave front advancing with the velocity of light. Such a surface will be called the front for brevity.

If the space-time

$$x = (x^0, x^1, x^2, x^3), \tag{2.10}$$

then, the light front time is defined as

$$x^+ = x^0 + x^3, \tag{2.11}$$

where x^0 is the conventional time and x^3 is the third component in the three dimensional coordinate space. And the third component of light front coordinate space is defined as

$$x^- = x^0 - x^3. \tag{2.12}$$

In analogy with the light front space-time variables, we define the longitudinal momentum

$$k^+ = k^0 + k^3, \tag{2.13}$$

and light front energy

$$k^- = k^0 - k^3. \tag{2.14}$$

The relation between light front momentum and light front energy is given by

$$k^- = \frac{k_\perp^2 + m^2}{k^+}. \tag{2.15}$$

Using the light front coordinates, we have

$$x\cdot y = \frac{1}{2}x^+y^- + \frac{1}{2}x^-y^+ - x^\perp y^\perp. \tag{2.16}$$

In light front coordinates, metric tensor $g^{+-} = g^{-+} = 2$, $g^{11} = g^{22} = -1$. Further, we have $g_{+-} = g_{-+} = \frac{1}{2}$.

The light front derivatives are given by

$$\begin{aligned} \partial_+ &= \frac{\partial}{\partial x^+} = \frac{1}{2}\partial^-, \\ \partial_- &= \frac{\partial}{\partial x^-} = \frac{1}{2}\partial^+, \\ \partial^i_\perp &= \frac{\partial}{\partial x^i}. \end{aligned} \tag{2.17}$$

The dot product of any two four-vectors, A and B, is then given by

$$A\cdot B = \frac{1}{2}(A^+B^- + A^-B^+) - A_\perp\cdot B_\perp. \tag{2.18}$$

2.2.2 Light front form

In a covariant theory, time and space are different aspects of four-dimensional space-time and the operators are functions of time and space. However, one can generalize the concepts of space and time to achieve alternative schemes in which the operators are the functions of the new defined "space-time". The requirement of the reparametrization is that the inverse transformation exists and different forms of reparametrization are not accessible by Lorentz transformation. Dirac [12] proved that there are no more than three different parametrizations: the instant form, the point form and the front form. The instant form is the conventional one we are familiar where the initial time is $t = 0$. In the point form the hypersphere on which one sets the "initial conditions" at the same "initial time" has a shape of a hyperboloid. In the front from, the hypersphere is a tangent plane to the light cone.

The three forms of Hamiltonian dynamics are shown in Fig. 2.1.

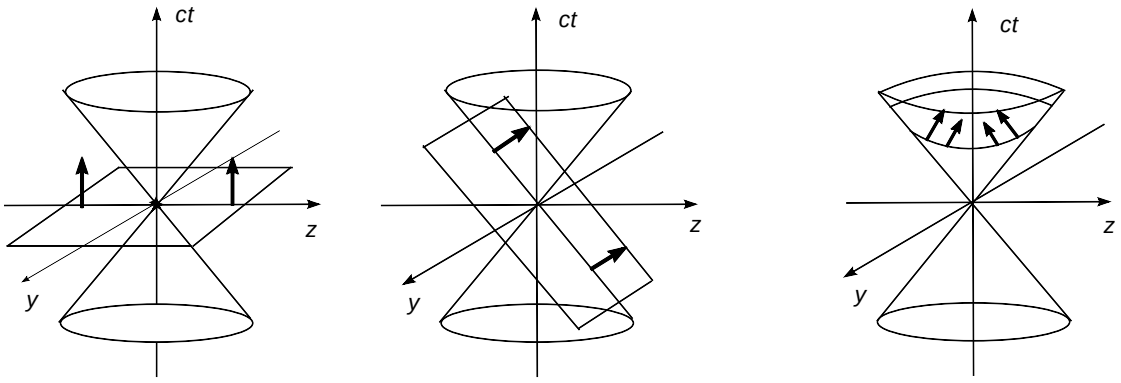

Figure 2.1 Three forms of Hamiltonian dynamics(from left to right): the instant form; the front form; the point form. In the instant form, the hypersphere where one quantizes the theory at the same initial "time" is a the plane with $x^0 = 0$. In the front form, the hypersphere is the plane with $x^0 + x^3 = 0$. And in the point form, the hypersphere is a hyperboloid.

2.2.3 The Poincaré symmetries in the front form

The Poincaré symmetries involve the generators which satisfy the relationships:

$$\begin{aligned}
&[P^\mu, P^\nu] = 0, \\
&[M^{\mu\nu}, P^\rho] = i(-g^{\mu\rho}P^\nu + g^{\nu\rho}P^\mu), \\
&[m^{\mu\nu}, M^{\rho\sigma}] = i(-g^{\mu\rho}M^{\nu\sigma} + g^{\nu\rho}M^{\mu\sigma} - g^{\mu\sigma}M^{\rho\nu} + g^{\nu\sigma}M^{\rho\mu}),
\end{aligned} \tag{2.19}$$

where P^μ is momentum four-vector, $M^{\mu\nu}$ is the angular momentum tensor and $g^{\mu\nu}$ is the metric tensor.

In the instant form, the rotational and boost operators, J^i and K^i, are given as $M_{ij} = i\epsilon_{ijk}J^k$ and $M^{0i} = K^i$ which satisfy

$$\begin{aligned}
\left[J^i, J^j\right] &= -i\epsilon_{ijk}J^k, \\
\left[J^i, K^j\right] &= i\epsilon_{ijk}K^k, \\
\left[K^i, K^j\right] &= -i\epsilon_{ijk}K^k,
\end{aligned} \tag{2.20}$$

where ϵ_{ijk} is 1 if the space-like indices ijk are in cyclic order, and zero otherwise.

In light front form, the boost and rotational operators are defined by

$$K^3 = -12M^{+-}, E^i = M^{+i},$$
$$J^3 = M^{12}, F^i = M^{-i}. \tag{2.21}$$

2.2.4 Why adopt the light front form?

Once we obtain the light front Hamiltonian, the problem of computing the eigenvalues and the corresponding wavefunctions can be reduced to solving the Hamiltonian eigenvalue problem with similarities (and differences) to the one encountered in non-relativistic many-body theory. The eigenstate of the light font Hamiltonian satisfies $(H_{LF} - M^2)|M\rangle = 0$ where $H_{LF} = P^-P^+ - P_\perp^2$. Projecting the Hamiltonian eigenvalue equation onto the various Fock-space states results in an infinite number of coupled integral eigenvalue equations which must be truncated to obtain numerical solutions. Equivalently, we can expand the eigenfunctions in a finite Fock-space basis and diagonalize H in that basis to obtain the eigenvalues and eigenfunctions.

In light front, the vacuum has eigenvalue 0 when $P_\perp$ and P^+ act on it:

$$P_\perp|0\rangle = 0,$$
$$P^+|0\rangle = 0. \tag{2.22}$$

The the light front momentum is nonnegative which is a key difference between light front quantization and ordinary equal time quantization where the momentum can be negative. Therefore in equal time quantization, the vacuum of the full Hamiltonian can be filled with an arbitrary number of particle and antiparticle pairs or quantum fluctuations, which has been shown in Eqn. (2.7). However in light front quantization each of the particles (neglecting zero modes which are discussed below) must carry some positive light front momentum and cannot exist in the vacuum state. Consequently, the vacuum of the free Hamiltonian is also the exact eigenstate of the full Hamiltonian. Specially in QCD even though the light front vacuum is potentially more complicated due to the possible filling with zero momentum massless gluons (occupants of the zero mode mentioned above), the physical vacuum is still simpler in light

front form than that in instant time since no quarks with finite mass can be present in the vacuum state.

2.3 From QCD Lagrangian to light front QCD Hamiltonian

In Chapter 1, the QCD Lagrangian is given by Eqn. (1.11). From Eqn. (1.11), the equations of motion for ψ and A^a_μ are given by

$$(i\gamma_\mu\partial^\mu - m + g\gamma_\mu A^\mu)\psi(x) = 0, \tag{2.23}$$

$$\partial_\mu F^{\mu\nu}_a + gf^{abc}A_{b\mu}F^{\mu\nu}_c + g\bar{\psi}\gamma^\nu t^a\psi = 0. \tag{2.24}$$

In order to obtain the Hamiltonian of QCD, we need to obtain the canonical momentum from the Lagrangian. The canonical momentum of A^a_μ is given by

$$(\pi_A)^\mu_a(x) = \frac{\partial\mathcal{L}}{\partial(\partial^- A_{a\mu})} = -\frac{1}{2}F^{+\mu}_a(x). \tag{2.25}$$

And the canonical momentum of ψ is given by

$$\pi_\psi(x) = \frac{\partial\mathcal{L}}{\partial(\partial^-\psi)} = \frac{1}{2}\bar{\psi}\gamma^+. \tag{2.26}$$

By using light front coordinates, Eqn. (2.23) can be written as

$$(i\partial^- + gt^a A^-_a)\psi_+ = (i\alpha_\perp\cdot D_\perp + \beta m)\psi_-, \tag{2.27}$$

$$(i\partial^+ + gt^a A^-_a)\psi_- = (i\alpha_\perp\cdot D_\perp + \beta m)\psi_+, \tag{2.28}$$

where we denote $\alpha_\perp = \gamma^0\gamma_\perp$, $\beta = \gamma^0$ and the quark fields $\psi(x)$ can be decomposed into $\psi(x) = \psi_+(x) + \psi_-(x)$ with $\psi_+(x) = \frac{1}{2}\gamma^0\gamma^\pm\psi(x)$. From the two equations above, we can see that ψ_- is a constraint field which can be expressed in terms of ψ_+ field:

$$\psi_- = \frac{1}{i\partial^+}(i\alpha_\perp\cdot D_\perp + \beta m)\psi_+. \tag{2.29}$$

and in the light front gauge $A^+_a = 0$, A^-_a is not an independent field and can be expressed in terms of the two transverse components A^i_a from the equation of motion:

$$\frac{1}{2}(\partial^+)^2 A^-_a = \partial^+\partial^i A^i_a + gf^{abc}A^i_b\partial^+ A^i_c + 2\psi^\dagger_+ t^a\psi_+. \tag{2.30}$$

Once we have the canonical momentum, the Light front QCD (LFQCD) Hamiltonian density is given by

$$\begin{aligned}\mathcal{H} &= \frac{1}{2}(\partial^i A_a^j)^2 + g f^{abc} A_a^i A_b^j \partial^i A_c^j + \frac{g^2}{4} f^{abc} f^{ade} A_b^i A_c^j A_d^i A_e^j \\ &+[\psi_+^\dagger \{\alpha_\perp \cdot (i\partial_\perp + gA_\perp) + \beta m\}(\frac{1}{i\partial^+})\{\alpha_\perp \cdot (i\partial_\perp + gA_\perp) + \beta m\}\psi_+] \\ &+g\partial^i A_a^i (\frac{1}{\partial^+})(f^{abc} A_b^i \partial^+ A_c^i + 2\psi_+^\dagger t^a \psi_+) \\ &+\frac{g^2}{2}(\frac{1}{\partial^+})(f^{abc} A_b^i \partial^+ A_c^i + 2\psi_+^\dagger t^a \psi_+)(\frac{1}{\partial^+})(f^{abc} A_b^i \partial^+ A_c^i + 2\psi_+^\dagger t^a \psi_+), \end{aligned} \tag{2.31}$$

where $\frac{1}{\partial^+}$ is defined by

$$\frac{1}{\partial^+} f(x^-) = \frac{1}{4}\int dy^- \epsilon(x^- - y^-) f(y^-), \tag{2.32}$$

and $\epsilon(x) = \theta(x) - \theta(-x)$. $\theta(x)$ is the step function which is equal to 0 when $x < 0$ and 1 when $x \geq 0$.

Once we have the LFQCD Hamiltonian, we can express it in terms of two-component field. To do so, we need to introduce the following γ matrices:

$$\gamma^0 = \begin{pmatrix} 0 & -i \\ i & 0 \end{pmatrix}, \gamma^3 = \begin{pmatrix} 0 & i \\ i & 0 \end{pmatrix}, \gamma^i = \begin{pmatrix} -i\epsilon^{ij}\sigma_j & 0 \\ 0 & i\epsilon^{ij}\sigma_j \end{pmatrix}, \tag{2.33}$$

where ϵ^{ij} is 1 when indices ij are in cyclic order and the light front quark fields have the two-component form:

$$\psi = \begin{pmatrix} \varphi \\ \nu \end{pmatrix}, \psi_+ = \begin{pmatrix} \varphi \\ 0 \end{pmatrix}, \psi_- = \begin{pmatrix} 0 \\ \nu \end{pmatrix} = \begin{pmatrix} 0 \\ \frac{1}{i\partial^+}(\hat{\sigma}^i(i\partial^i + gA^i) + im)\varphi \end{pmatrix}, \tag{2.34}$$

where $\varphi(x)$ is a two-component spinor field and σ_i are Pauli matrices which are given as follows

$$\sigma_1 = \begin{pmatrix} 0 & 1 \\ 1 & 0 \end{pmatrix}, \sigma_1 = \begin{pmatrix} 0 & -i \\ i & 0 \end{pmatrix}, \sigma_3 = \begin{pmatrix} 1 & 0 \\ 0 & -1 \end{pmatrix}. \tag{2.35}$$

Here $\hat{\sigma}^1 = \sigma^2$ and $\hat{\sigma}^2 = -\sigma^1$.

In the two-component form, the LFQCD Hamiltonian Eqn. (2.31) can be written as

$$\mathcal{H} = \mathcal{H}_0 + \mathcal{H}_{int}, \tag{2.36}$$

where

$$\mathcal{H}_0 = \frac{1}{2}(\partial^i A_a^j)(\partial^i A_a^j) + \varphi^\dagger(\frac{-\nabla^2 + m^2}{i\partial^+})\varphi, \tag{2.37}$$

$$\mathcal{H}_{int} = \mathcal{H}_{qqg} + \mathcal{H}_{ggg} + \mathcal{H}_{qqgg} + \mathcal{H}_{qqqq} + \mathcal{H}_{gggg}, \tag{2.38}$$

and

$$\begin{aligned}\mathcal{H}_{qqg} &= g\varphi^\dagger\{-2(\frac{1}{\partial^+})(\partial_\perp\cdot A_\perp) + \hat{\sigma}_\perp\cdot A_\perp(\frac{1}{\partial^+})(\hat{\sigma}_\perp\cdot\partial_\perp + m) \\ &\quad +(\frac{1}{\partial^+})(\hat{\sigma}_\perp\cdot\partial_\perp - m)\hat{\sigma}_\perp\cdot A_\perp\}\varphi,\end{aligned} \tag{2.39}$$

$$\mathcal{H}_{ggg} = gf^{abc}\{\partial^i A_a^j A_b^i A_c^j + (\partial^i A_a^i)(\frac{1}{\partial^+})(A_b^j\partial^+ A_c^j)\}, \tag{2.40}$$

$$\begin{aligned}\mathcal{H}_{qqgg} &= g^2\{\varphi^\dagger\hat{\sigma}_\perp\cdot A_\perp\}(\frac{1}{i\partial^+})\hat{\sigma}_\perp\cdot A_\perp\}\varphi \\ &\quad +2(\frac{1}{\partial^+})(f^{abc}A_b^j\partial^+ A_c^j)(\frac{1}{\partial^+})(\varphi^\dagger T^a\varphi)\} \\ &= \mathcal{H}_{qqgg1} + \mathcal{H}_{qqgg2},\end{aligned} \tag{2.41}$$

$$\mathcal{H}_{qqqq} = 2g^2\{(\frac{1}{\partial^+})(\varphi^\dagger T^a\varphi)(\frac{1}{\partial^+})(\varphi^\dagger T^a\varphi)\}, \tag{2.42}$$

$$\begin{aligned}\mathcal{H}_{gggg} &= \frac{g^2}{4}f^{abc}f^{ade}\{A_b^i A_c^j A_d^i A_e^j + 2(\frac{1}{\partial^+})(A_b^i\partial^+ A_c^i)(\frac{1}{\partial^+})(A_d^j\partial^+ A_e^j)\} \\ &= \mathcal{H}_{gggg1} + \mathcal{H}_{gggg2}.\end{aligned} \tag{2.43}$$

In this section, we have obtained the LFQCD Hamiltonian from the LFQCD Lagrangian. The $\mathcal{H}_{int}$ is given in terms of Eqn. (2.39), Eqn. (2.40), Eqn. (2.41), Eqn. (2.42), Eqn. (2.43). In the next section, we will quantize the fields and find the light front Hamiltonian diagrammatic rules corresponding to $\mathcal{H}_{int}$.

2.4 Light front Hamiltonian diagrammatic rules

In this section, we present the light front Hamiltonian diagrammatic rules. Before we obtain the Hamiltonian diagrammatic rules, we list some basic results which will be used in

the following calculation. At first, we need to adopt an expansion of gauge field which we take in the conventional form for the present :

$$A^i(x) = \sum_\lambda \int \frac{dk^+ d^2k^\perp}{2(2\pi)^3 k^+}[a(k,\lambda)\epsilon^i_\lambda e^{-ik\cdot x} + a^+(k,\lambda)(\epsilon^i_\lambda)^\star e^{ik\cdot x}], \tag{2.44}$$

where ϵ^i_λ is the gauge field polarization vector: $\epsilon^i_1 = \frac{1}{\sqrt{2}}(1,i)$, $\epsilon^i_{-1} = \frac{1}{\sqrt{2}}(1,-i)$.

Similarly, we expand the fermion field:

$$\varphi(x) = \sum_\lambda \chi_\lambda \int \frac{dk^+ d^2k^\perp}{2(2\pi)^3\sqrt{k^+}}[b(k,\lambda)e^{-ik\cdot x} + d^+(k,-\lambda)e^{ik\cdot x}], \tag{2.45}$$

where χ_λ is the spin eigenstate:

$$\chi_{1/2} = \begin{pmatrix} 1 \\ 0 \end{pmatrix}, \chi_{-1/2} = \begin{pmatrix} 0 \\ 1 \end{pmatrix}. \tag{2.46}$$

From the commutation relation for bosonic fields and anticommutation relation for fermionic fields, we have

$$[a(k_1,\lambda_1), a^+(k_2,\lambda_2)] = 2(2\pi)^3 k_1^+ \delta^3(k_1 - k_2)\delta_{\lambda_1\lambda_2}, \tag{2.47}$$

$$\{b(k,\lambda_1), b^+(p,\lambda_2)\} = 2(2\pi)^3 p^+ \delta^3(k-p)\delta_{\lambda_1\lambda_2}, \tag{2.48}$$

$$\{d(k,\lambda_1), d^+(p,\lambda_2)\} = 2(2\pi)^3 p^+ \delta^3(k-p)\delta_{\lambda_1\lambda_2}. \tag{2.49}$$

2.4.1 Diagrammatic rule for interaction Hamiltonian $\mathcal{H}_{qqg}$

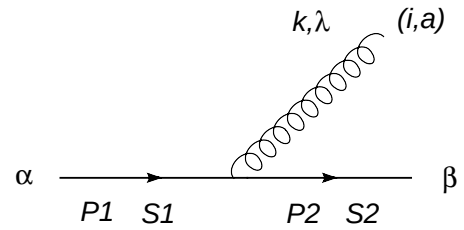

Figure 2.2 $\mathcal{H}_{qqg}$: quark to quark and gluon transition term in the interaction Hamiltonian.

The quark to quark and gluon transition term in the interaction Hamiltonian $\mathcal{H}_{qqg}$ is given by Eqn. (2.39). To obtain the diagrammatic rule for this interaction, we define an initial state

which is $|p_1, s_1\rangle$ and a final state which is $|p_2, s_2; k, \lambda\rangle$. A diagram to describe this process is given by Fig. 2.2.

In Eqn. (2.39), when the term $\varphi^\dagger\{(\frac{1}{\partial^+})(\partial\cdot A_\perp)\varphi$ is sandwiched between the initial state and final state, we have

$$\begin{aligned}
& \langle p_2, s_2; k, \lambda|\varphi^\dagger(\frac{1}{\partial^+})(\partial_\perp \cdot A_\perp)\varphi|p_1, s_1\rangle \\
= \;& \langle 0|a(k,\lambda)b(p_2,s_2)\varphi^\dagger(\frac{1}{\partial^+})(\partial_\perp \cdot A_\perp)\varphi b^+(p_1,s_1)|0\rangle \\
= \;& \chi^+_{s2}\chi_{s1}\sqrt{p_1^+}\sqrt{p_2^+}\langle 0|a(k,\lambda)e^{ip_2\cdot x}(\frac{1}{\partial^+})(\partial_\perp \cdot A_\perp)e^{-ip_1\cdot x}|0\rangle \\
= \;& \chi^+_{s2}\chi_{s1}\sqrt{p_1^+}\sqrt{p_2^+}(ik^i)(\epsilon^i_\lambda)^\star\frac{-i}{k^+}\langle 0|e^{i(p_2+k_1-p_1)\cdot x}|0\rangle, \qquad (2.50)
\end{aligned}$$

and when the term $\varphi^\dagger\hat{\sigma}_\perp \cdot A_\perp(\frac{1}{\partial^+})(\hat{\sigma}_\perp \cdot \partial_\perp + m)\varphi$ is sandwiched between the initial state and final state, we have

$$\begin{aligned}
& \langle p_2, s_2; k, \lambda|\varphi^\dagger\hat{\sigma}_\perp \cdot A_\perp(\frac{1}{\partial^+})(\hat{\sigma}_\perp \cdot \partial_\perp + m)\varphi|p_1, s_1\rangle \\
= \;& \chi^+_{s2}\chi_{s1}\sqrt{p_1^+}\sqrt{p_2^+}\langle 0|a(k,\lambda)e^{ip_2\cdot x}\hat{\sigma}_\perp \cdot A_\perp(\frac{1}{\partial^+})(\hat{\sigma}_\perp \cdot \partial_\perp + m)e^{-ip_1\cdot x}|0\rangle \\
= \;& \chi^+_{s2}\chi_{s1}\sqrt{p_1^+}\sqrt{p_2^+}\hat{\sigma}_i \cdot (\epsilon^i_\lambda)^\star(-i\hat{\sigma}_j \cdot p_1^j + m)\frac{i}{p_1^+}\langle 0|e^{i(p_2+k_1-p_1)\cdot x}|0\rangle, \qquad (2.51)
\end{aligned}$$

and, finally, when the last term $\varphi^\dagger(\frac{1}{\partial^+})(\hat{\sigma}_\perp \cdot \partial_\perp - m)\hat{\sigma}_\perp \cdot A_\perp\varphi$ is sandwiched between the initial state and final state, we have

$$\begin{aligned}
& \langle p_2, s_2; k, \lambda|\varphi^\dagger(\frac{1}{\partial^+})(\hat{\sigma}_\perp \cdot \partial_\perp - m)\hat{\sigma}_\perp \cdot A_\perp\varphi|p_1, s_1\rangle \\
= \;& \chi^+_{s2}\chi_{s1}\sqrt{p_1^+}\sqrt{p_2^+}\langle 0|e^{ip_2\cdot x}(\frac{1}{\partial^+})(\hat{\sigma}_\perp \cdot \partial_\perp - m)\hat{\sigma}_i \cdot (\epsilon^i_\lambda)^\star e^{i(k_1-p_1)\cdot x}|0\rangle \\
= \;& \chi^+_{s2}\chi_{s1}\sqrt{p_1^+}\sqrt{p_2^+}\frac{-i}{k^+ - p_1^+}(-i\hat{\sigma}_i \cdot (p_1^i - k^i) - m)\hat{\sigma}_i \cdot (\epsilon^i_\lambda)^\star\langle 0|e^{i(p_2+k_1-p_1)\cdot x}|0\rangle. \qquad (2.52)
\end{aligned}$$

Therefore, when we combine them together, we obtain the diagrammatic rule for the interaction Hamiltonian $\mathcal{H}_{qqg}$:

$$\begin{aligned}
& \langle p_2, s_2; k, \lambda|\mathcal{H}_{qqg}|p1, s1\rangle \\
= \;& -g\chi^+_{s2}\sqrt{p_1^+}\sqrt{p_2^+}\{-2\frac{k^i}{k^+} - \hat{\sigma}_i\frac{(\hat{\sigma}_i \cdot p_1^i + im)}{p_1^+} - \frac{(\hat{\sigma}_i \cdot p_2^i - im)}{p_1^+ - k^+}\hat{\sigma}_i\}(\epsilon^i_\lambda)^\star\chi_{s1}. \qquad (2.53)
\end{aligned}$$

Note: If we change final quark with momentum p_2 into initial antiquark with same momentum, we found the result is the same except that the 4-momentum conservation will be $p_1 + p_2 = k$.

2.4.2 Diagrammatic rule for interaction Hamiltonian $\mathcal{H}_{ggg}$

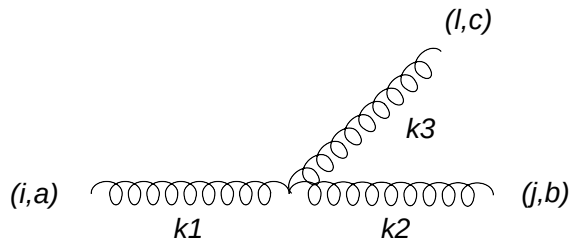

Figure 2.3 $\mathcal{H}_{ggg}$: three-gluon interaction Hamiltonian

The Hamiltonian of three-gluon interaction $\mathcal{H}_{ggg}$ is given by Eqn. (2.40). The initial state is $|k_1, i\rangle$ and the final state is $|k_2, j; k_3, l\rangle$.

In terms of the gauge field expansion in Eqn. (2.44), we have

$$\begin{aligned}
\partial^m A^n_{a'} A^m_{b'} A^n_{c'} \quad = \quad & \int \frac{dp_1^+ d^2p_1^\perp}{2(2\pi)^3 p_1^+} \frac{dp_2^+ d^2p_2^\perp}{2(2\pi)^3 p_2^+} \frac{dp_3^+ d^2p_3^\perp}{2(2\pi)^3 p_3^+} \\
& \{[a(p_1)\epsilon^n_{a'} e^{-ip_1\cdot x}(-ip_1^m) + a^+(p_1)(\epsilon^n_{a'})^\star e^{ip_1\cdot x}(ip_1^m)] \\
& [a(p_2)\epsilon^m_{b'} e^{-ip_2\cdot x} + a^+(p_2)(\epsilon^m_{b'})^\star e^{ip_2\cdot x}] \\
& [a(p_3)\epsilon^n_{c'} e^{-ip_3\cdot x} + a^+(p_3)(\epsilon^n_{c'})^\star e^{ip_3\cdot x}]\}. \qquad (2.54)
\end{aligned}$$

From the expression above, we know that only the following operators have a contribution for the given initial state and the final state:

$$\begin{aligned}
& a(p_1)a^+(p_2)a^+(p_3)\epsilon^n_{a'}(\epsilon^m_{b'})^\star(\epsilon^n_{c'})^\star(-ip_1^m)e^{-i(p_1-p_2-p_3)\cdot x} \\
+ \quad & a^+(p_1)a(p_2)a^+(p_3)(\epsilon^n_{a'})^\star\epsilon^m_{b'}(\epsilon^n_{c'})^\star(ip_1^m)e^{i(p_1-p_2+p_3)\cdot x} \\
+ \quad & a^+(p_1)a^+(p_2)a(p_3)(\epsilon^n_{a'})^\star(\epsilon^m_{b'})^\star\epsilon^n_{c'}(ip_1^m)e^{i(p_1+p_2-p_3)\cdot x}, \qquad (2.55)
\end{aligned}$$

and after we sandwich these operators between the given initial state and the final state, we have

$$\begin{aligned}
& \langle k_2, j; k_3, l|\partial^m A^n_{a'} A^m_{b'} A^n_{c'}|k_1, i\rangle \\
= \quad & \delta_{p_1k_1}\delta_{p_2k_2}\delta_{p_3k_3}\delta_{ni}\delta_{mj}\delta_{nl}\delta_{a'a}\delta_{b'b}\delta_{c'c}(-ik_1^j) \\
& +\delta_{p_1k_1}\delta_{p_2k_3}\delta_{p_3k_2}\delta_{ni}\delta_{ml}\delta_{nj}\delta_{a'a}\delta_{b'c}\delta_{c'b}(-ik_1^l)
\end{aligned}$$

$$
\begin{aligned}
&+\delta_{p_2k_1}\delta_{p_1k_2}\delta_{p_3k_3}\delta_{mi}\delta_{nj}\delta_{nl}\delta_{b'a}\delta_{a'b}\delta_{c'c}(ik_2^i)\\
&+\delta_{p_2k_1}\delta_{p_1k_3}\delta_{p_3k_2}\delta_{mi}\delta_{nl}\delta_{nj}\delta_{b'a}\delta_{a'c}\delta_{c'b}(ik_3^i)\\
&+\delta_{p_3k_1}\delta_{p_1k_2}\delta_{p_2k_3}\delta_{ni}\delta_{nj}\delta_{ml}\delta_{c'a}\delta_{a'b}\delta_{b'c}(ik_2^l)\\
&+\delta_{p_3k_1}\delta_{p_1k_3}\delta_{p_2k_2}\delta_{ni}\delta_{nl}\delta_{mj}\delta_{c'a}\delta_{a'c}\delta_{b'b}(ik_3^j). \qquad (2.56)
\end{aligned}
$$

Therefore, for the first term of $\mathcal{H}_{ggg}$, we have

$$
\begin{aligned}
& gf^{a'b'c'}\langle k_2,j;k_3,l|\partial^m A^n_{a'}A^m_{b'}A^n_{c'}|k_1,i\rangle\\
= \;& -igf^{abc}\{(k_1+k_3)^j\delta_{il}-(k_1+k_2)^l\delta_{ij}+(k_2-k_3)^i\delta_{lj}\}. \qquad (2.57)
\end{aligned}
$$

We can use the same procedure to calculate the second term of $\mathcal{H}_{ggg}$, which is given by

$$
\begin{aligned}
& gf^{a'b'c'}\langle k_2,j;k_3,l|\partial^m A^m_{a'}(\frac{1}{\partial^+})(A^n_{b'}\partial^+A^n_{c'})|k_1,i\rangle\\
= \;& igf^{abc}\{k_2^j\frac{k_1^+ + k_3^+}{k_1^+ - k_3^+}\delta_{il}-k_1^i\frac{k_3^+ - k_2^+}{k_2^+ + k_3^+}\delta_{lj}+k_3^l\frac{-k_1^+ - k_2^+}{k_1^+ - k_2^+}\delta_{ij}\}. \qquad (2.58)
\end{aligned}
$$

Therefore, we have

$$
\begin{aligned}
& \langle k_2,j;k_3,l|\mathcal{H}_{ggg}|k_1,i\rangle\\
= \;& -igf^{abc}\{[(k_2-k_3)^i-\frac{k_1^i}{k_1^+}(k_2^+-k_3^+)]\delta_{jl}+[(k_1+k_3)^j-\frac{k_2^j}{k_2^+}(k_1^++k_3^+)]\delta_{il}\\
& +[-(k_1+k_2)^l+\frac{k_3^l}{k_3^+}(k_1^++k_2^+)]\delta_{ij}\}. \qquad (2.59)
\end{aligned}
$$

2.4.3 Diagrammatic rule for interaction Hamiltonian $\mathcal{H}_{qqgg1}$

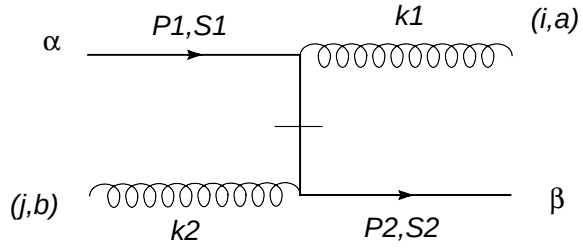

Figure 2.4 $\mathcal{H}_{qqgg1}$

From Eqn. (2.41), the Hamiltonian $\mathcal{H}_{qqgg1}$ corresponding to the diagram above is given by

$$
\mathcal{H}_{qqgg1} = g^2\varphi^\dagger\hat{\sigma}_\perp\cdot A_\perp(\frac{1}{i\partial^+})\hat{\sigma}_\perp\cdot A_\perp\varphi. \qquad (2.60)
$$

The initial state is $|p_1, s_1; k_2\rangle$ and the final state is $|p_2, s_2; k_1\rangle$.

In terms of the field expansions given in Eqn.(2.44) and Eqn.(2.45), we have

$$\begin{aligned} & g^2\langle p_2, s_2; k_1|\varphi^\dagger\hat{\sigma}_\perp \cdot A_\perp(\frac{1}{i\partial^+})\hat{\sigma}_\perp \cdot A_\perp\varphi|p_1, s_1; k_2\rangle \\ = \; & g^2\langle p_2, s_2|\varphi^\dagger\hat{\sigma}_\perp \cdot A_\perp|k_2\rangle\langle k_1|(\frac{1}{i\partial^+})\hat{\sigma}_\perp \cdot A_\perp\varphi|p_1, s_1\rangle \\ = \; & g^2\sqrt{p_1^+}\sqrt{p_2^+}\chi^+_{s_2}\frac{\hat{\sigma}_j\hat{\sigma}_i}{p_1^+ - k_1^+}\chi_{s_1}(\epsilon^i)^\star\epsilon^j. \end{aligned} \tag{2.61}$$

2.4.4 Diagrammatic rule for interaction Hamiltonian $\mathcal{H}_{qqgg2}$

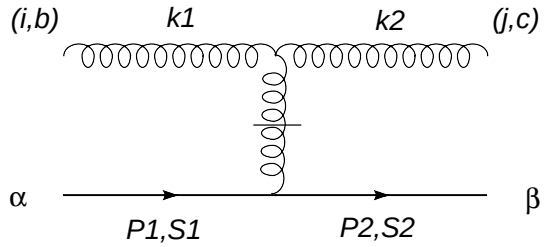

Figure 2.5 $\mathcal{H}_{qqgg2}$

From Eqn. (2.41), the Hamiltonian $\mathcal{H}_{qqgg2}$ corresponding to the diagram above is given by

$$\mathcal{H}_{qqgg2} = 2g^2(\frac{1}{\partial^+})(f^{abc}A^i_b\partial^+A^i_c)(\frac{1}{\partial^+})(\varphi^\dagger T^a\varphi). \tag{2.62}$$

The initial state is $|p_1, s_1; k_1, i\rangle$ and the final state is $|p_2, s_2; k_2, j\rangle$.

After we expand the operator $A^n_{b'}\partial^+A^n_{c'}$, only the following terms have the contribution for the given initial state and final state:

$$a(k^{'})a^+(k'')\epsilon^n_{b'}(\epsilon^n_{c'})^\star(i(k'')^+) + a^+(k^{'})a(k'')(\epsilon^n_{b'})^\star\epsilon^n_{c'}(-i(k'')^+). \tag{2.63}$$

Therefore, the diagrammatic rule for the interaction Hamiltonian $\mathcal{H}_{qqgg2}$ is given by

$$\begin{aligned} & \langle p_2, s_2; k_2, j|\mathcal{H}_{qqgg2}|p_1, s_1; k_1, i\rangle \\ = \; & 2g^2 f^{a^{'}b^{'}c^{'}}\langle p_2, s_2|(\frac{1}{\partial^+})(\varphi^\dagger T^{a^{'}}\varphi)|p_1, s_1\rangle\langle k_2, j|(\frac{1}{\partial^+})A^n_{b'}\partial^+A^n_{c'})|k_1, i\rangle \\ = \; & 2g^2 f^{a^{'}b^{'}c^{'}}\frac{i}{p_1^+ - p_2^+}\sqrt{p_1^+}\sqrt{p_2^+}(T^{a^{'}}_{\beta\alpha}\chi^+_{s_2}\chi_{s_1}\delta_{a'a}) \\ & (\delta_{k'k_1}\delta_{k''k_2}\delta_{ni}\delta_{nj}\delta_{b'b}\delta_{c'c}\frac{i}{k_1^+ - k_2^+}(ik_2^+) \end{aligned}$$

$$
\begin{aligned}
& +\delta_{k^{"}k_1}\delta_{k'k_2}\delta_{ni}\delta_{nj}\delta_{c'b}\delta_{b'c}\frac{i}{k_1^+-k_2^+}(-ik_2^+)) \\
= \quad & -2g^2\sqrt{p_1^+}\sqrt{p_2^+}f^{abc}iT^a_{\beta\alpha}\chi^+_{s_2}\chi_{s_1}\frac{k_1^++k_2^+}{(k_1^+-k_2^+)^2}\delta_{ij}\epsilon^i(\epsilon^j)^\star. \qquad (2.64)
\end{aligned}
$$

2.4.5 Diagrammatic rule for interaction Hamiltonian $\mathcal{H}_{qqqq}$

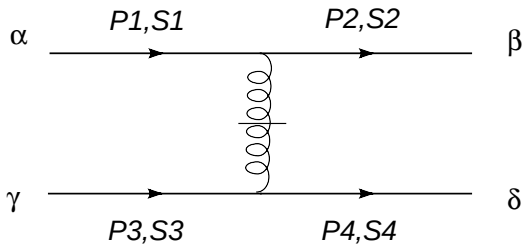

Figure 2.6 $\mathcal{H}_{qqqq}$: four-quark interaction.

The Hamiltonian corresponding to the diagram above is given by Eqn. (2.42). The initial state is $|p_1,s_1;p_3,s_3\rangle$ and the final state is $|p_2,s_2;p_4,s_4\rangle$.

$$
\begin{aligned}
& \langle p_2,s_2;p_4,s_4|\mathcal{H}_{qqqq}|p_1,s_1;p_3,s_3\rangle \\
= \quad & 2g^2\sqrt{(p_1^+p_2^+p_3^+p_4^+)}T^a_{\beta\alpha}T^a_{\delta\gamma}\frac{i}{p_1^+-p_2^+}\frac{i}{p_3^+-p_4^+}\chi^+_{s_2}\chi_{s_1}\chi^+_{s_4}\chi_{s_3} \\
= \quad & 2g^2\sqrt{(p_1^+p_2^+p_3^+p_4^+)}T^a_{\beta\alpha}T^a_{\delta\gamma}\frac{1}{(p_1^+-p_2^+)^2}\chi^+_{s_2}\chi_{s_1}\chi^+_{s_4}\chi_{s_3}. \qquad (2.65)
\end{aligned}
$$

If we change the quarks with momentum p_3 and p_4 into antiquarks with the same momentum, we will have the same Hamiltonian $\mathcal{H}_{qqqq}$. However only these operators within Hamiltonian $\mathcal{H}_{qqqq}$ have the contributions to antiquarks instead of quarks:

$$
\begin{aligned}
(\frac{1}{\partial^+})(\varphi^\dagger\varphi)(\frac{1}{\partial^+})(\varphi^\dagger\varphi) \quad \rightarrow \quad & \frac{i}{k_2-k_1}\frac{i}{k_3-k_4}b^+(k_1,\lambda_1)b(k_2,\lambda_2)d(k_3,\lambda_3)d^+(k_4,\lambda_4) \\
& \frac{-i}{k_2+k_1}\frac{i}{k_3+k_4}b^+(k_1,\lambda_1)d^+(k_2,\lambda_2)d(k_3,\lambda_3)b(k_4,\lambda_4) \\
& \frac{i}{k_2+k_1}\frac{-i}{k_3+k_4}d(k_1,\lambda_1)b(k_2,\lambda_2)b^+(k_3,\lambda_3)d^+(k_4,\lambda_4) \\
& \frac{i}{k_1-k_2}\frac{-i}{k_3-k_4}d(k_1,\lambda_1)d^+(k_2,\lambda_2)b^+(k_3,\lambda_3)b(k_4,\lambda_4). \qquad (2.66)
\end{aligned}
$$

Then we have

$$\langle 0|b(p_2,s_2)d(p_4,s_4)\mathcal{H}_{qqqq}b^+(p_1,s_1)d^+(p_3,s_3)|0\rangle$$

$$
\begin{aligned}
&= 4g^2\sqrt{(p_1^+p_2^+p_3^+p_4^+)}T^a_{\beta\alpha}T^a_{\delta\gamma}\left(\frac{i}{p_1^+-p_2^+}\frac{i}{p_3^+-p_4^+}+\frac{i}{p_1^++p_3^+}\frac{-i}{p_2^++p_4^+}\right)\chi^+_{s_2}\chi_{s_1}\chi^+_{s_4}\chi_{s_3} \\
&= 4g^2\sqrt{(p_1^+p_2^+p_3^+p_4^+)}T^a_{\beta\alpha}T^a_{\delta\gamma}\left(\frac{1}{(p_1^+-p_2^+)^2}+\frac{1}{(p_1^++p_3^+)^2}\right)\chi^+_{s_2}\chi_{s_1}\chi^+_{s_4}\chi_{s_3}. \qquad (2.67)
\end{aligned}
$$

In the parenthesis of the expression above, the first term corresponds to the same diagram as Fig. 2.6 except that we have changed two quarks with momentum p_3 and p_4 into two antiquarks with the same momentum. However the second term in the parenthesis corresponds to the new diagram which is given by Fig. 2.7.

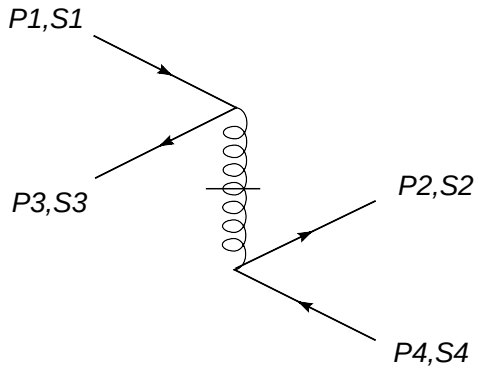

Figure 2.7 Additional new diagram corresponds to $\mathcal{H}_{q\bar{q}q\bar{q}}$

2.4.6 Diagrammatic rule for interaction Hamiltonian $\mathcal{H}_{gggg1}$

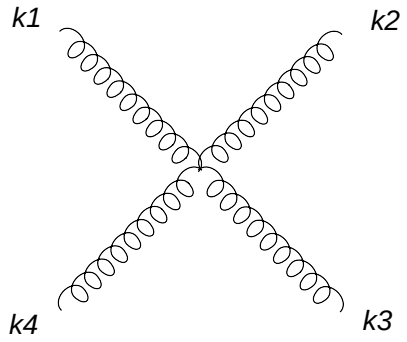

Figure 2.8 $\mathcal{H}_{gggg1}$

The Hamiltonian corresponding to Fig. 2.8 is given by

$$\mathcal{H}_{gggg1} = \frac{g^2}{4} f^{abc} f^{ade} A^i_b A^j_c A^i_d A^j_e. \tag{2.68}$$

The initial state is $|k_1; k_2; k_3; k_4\rangle$ and the final state is $|0\rangle$. Since final state gluons are identical particles, there are 4!=24 ways to eliminate initial states. The final result is given by

$$\langle 0|\mathcal{H}_{gggg1}|k_1; k_2; k_3; k_4\rangle = g^2\{f^{a_1a_2b} f^{a_3a_4b}[\delta_{i_1i_3}\delta_{i_2i_4} - \delta_{i_1i_4}\delta_{i_2i_3}] + (2 \to 3) + (2 \to 4)\}. \tag{2.69}$$

2.4.7 Diagrammatic rule for interaction Hamiltonian $\mathcal{H}_{gggg2}$

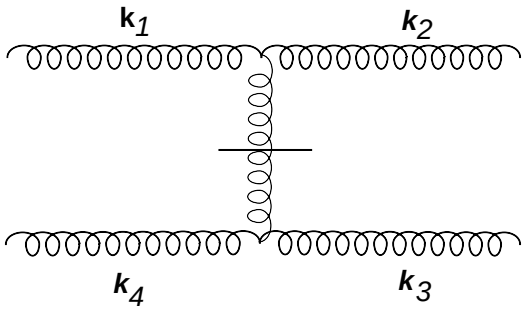

Figure 2.9 $\mathcal{H}_{gggg2}$

The Hamiltonian corresponding to Fig. 2.9 is given by

$$\mathcal{H}_{gggg2} = \frac{g^2}{2} f^{abc} f^{ade} (\frac{1}{\partial^+})(A^i_b \partial^+ A^i_c)(\frac{1}{\partial^+})(A^j_d \partial^+ A^j_e). \tag{2.70}$$

The initial state is $|k_1, i_1; k_4, i_4\rangle$ and the final state is $|k_2, i_2; k_3, i_3\rangle$. And

$$\begin{aligned} & \langle k_2, i_2|(\frac{1}{\partial^+})(A^i_b \partial^+ A^i_c)|k_1, i_1\rangle \\ = \; & \delta_{k'k_1}\delta_{k''k_2}\delta_{ii_1}\delta_{ii_2}\delta_{ba_1}\delta_{ca_2}\frac{i}{k_1^+ - k_2^+}(ik_2^+) \\ & +\delta_{k''k_1}\delta_{k'k_2}\delta_{ii_1}\delta_{ii_2}\delta_{ba_2}\delta_{ca_1}\frac{i}{k_1^+ - k_2^+}(-ik_2^+). \end{aligned} \tag{2.71}$$

Therefore

$$\begin{aligned} & f^{abc}\langle k_2, i_2|(\frac{1}{\partial^+})(A^i_b \partial^+ A^i_c)|k_1, i_1\rangle \\ = \; & if^{aa_1a_2}\frac{i(k_1^+ + k_2^+)}{k_1^+ - k_2^+}\delta_{i_1i_2}. \end{aligned} \tag{2.72}$$

We can follow a similar procedure to obtain

$$\begin{aligned} & f^{ade}\langle k_4, i_4|(\frac{1}{\partial^+})(A^j_d \partial^+ A^j_e)|k_3, i_3\rangle \\ = \; & if^{aa_4a_3}\frac{i(k_3^+ + k_4^+)}{k_4^+ - k_3^+}\delta_{i_3i_4}. \end{aligned} \tag{2.73}$$

Therefore,

$$\begin{aligned} & \langle k_2, i_2; k_3, i_3|\mathcal{H}_{gggg2}|k_1, i_1; k_4, i_4\rangle \\ = \; & g^2 f^{aa_1a_2}f^{aa_4a_3}\frac{(k_1^+ + k_2^+)(k_3^+ + k_4^+)}{(k_1^+ - k_2^+)(k_4^+ - k_3^+)}\delta_{i_1i_2}\delta_{i_3i_4}. \end{aligned} \tag{2.74}$$

Note that two final gluons can be exchanged. Therefore, if we exchange k_2 and k_3, we have

$$\begin{aligned} & \langle k_2, i_2; k_3, i_3|\mathcal{H}_{gggg2}|k_1, i_1; k_4, i_4\rangle \\ = \; & g^2 f^{aa_1a_3}f^{aa_4a_2}\frac{(k_1^+ + k_3^+)(k_2^+ + k_4^+)}{(k_1^+ - k_3^+)(k_4^+ - k_2^+)}\delta_{i_1i_3}\delta_{i_2i_4}. \end{aligned} \tag{2.75}$$

In addition, if we exchange k_1 and k_4, we have

$$\begin{aligned} & \langle k_2, i_2; k_3, i_3|\mathcal{H}_{gggg2}|k_1, i_1; k_4, i_4\rangle \\ = \; & g^2 f^{aa_4a_2}f^{aa_1a_3}\frac{(k_2^+ + k_4^+)(k_3^+ + k_1^+)}{(k_4^+ - k_2^+)(k_1^+ - k_3^+)}\delta_{i_4i_3}\delta_{i_2i_1}. \end{aligned} \tag{2.76}$$

Therefore, after we combine all the results together, we have

$$\begin{aligned} & \langle k_2, i_2; k_3, i_3|\mathcal{H}_{gggg2}|k_1, i_1; k_4, i_4\rangle \\ = \; & g^2\{f^{aa_1a_2}f^{aa_4a_3}\frac{(k_1^+ + k_2^+)(k_3^+ + k_4^+)}{(k_1^+ - k_2^+)(k_4^+ - k_3^+)}\delta_{i_1i_2}\delta_{i_3i_4} \\ & +(2 \to 3) + (1 \to 4)\}. \end{aligned} \tag{2.77}$$

CHAPTER 3. COLOR SINGLET STATES OF MULTIPARTON HADRONS

3.1 Introduction

Quarks and gluons have a novel degree of freedom called *color*. In color space, a quark has three colors and a gluon has eight colors. Free quarks and gluons have not been observed in nature, which implies the existence of the phenomena called confinement. Confinement dictates that what we can observe is colorless particles such as mesons and baryons where the Fock space components each have their color arranged so that that no net color remains. A meson has a leading Fock space component of one quark and one antiquark while a baryon has a leading Fock space component of three quarks. In order to know how quarks or antiquarks are arranged into the color singlet state for the meson and baryon, we need to consider how the algebra in color space can be used to provide color singlet states. The details about how to deal with color algebra is given in Appendix A. To obtain the multiparton hadrons, systems of mesons and baryons that can involve dynamic gluon configurations, we also need to construct the generic algebra in color space such that we can obtain singlet states of particles constructed from any arbitrary number of partons in principle. Here we take advantage of the global color operator F^2 which gives zero eigenvalue when it acts on arbitrary color singlet states and gives positive eigenvalues when it acts on arbitrary color non-singlet states [13] [14]. F^2 is defined as

$$F^2 = \sum_{i=1}^{8} F_i F_i, \tag{3.1}$$

where in the fundamental representation

$$F_i = \frac{1}{2}\lambda_i. \tag{3.2}$$

λ_i is one of 8 Gell-Mann matrices. In the adjoint representation

$$F_i = t_i, \tag{3.3}$$

$(t^b)_{ac} = if^{abc}$ in the adjoint representation.

In the following parts, we will obtain the color singlet states by using the operator F^2 when we consider systems of varying numbers of quarks and gluons. At first, we list all the states in the color space for the given number of the quarks and gluons - i.e. all partons have a specified color in each basis state and the full basis space (in color space) consists of all possible arrangements of single parton colors for that number of quarks and gluons. The color singlet state is the eigenstate of F^2 with zero eigenvalue which is the linear combination of some of these (possibly all of these) states in color space. When we obtain the representation of operator F^2 in color space, usually we will generate a very large matrix. In order to reduce the size of the matrix F^2, we can use two additional color operators T_3 and Y which are defined in the Appendix A and which will give zero when they act on the basis states which form the color singlet states. Therefore, we can initially employ these two operators to limit the multi-parton basis states in color space for the needed representation of F^2. Finally, we will diagonalize the resulting matrix of F^2 to obtain the states with zero eigenvalues (if any) which correspond to color singlet states for that specific assemblage of quarks and gluons.

In the following, we will consider a number of representative systems and find the color singlet states if they exist.

3.1.1 Mesons

It is well known that one quark and one antiquark can form only one color singlet state, which is an equally weighted combination of color and anticolor configurations. The operator F^2 acting on this color singlet state gives zero eigenvalue. On the other hand, F^2 gives positive eigenvalues when it acts on color non-singlet states of the quark plus antiquark system.

In order to obtain the matrix representation of F^2, we need to find out all the color configurations for one quark and one antiquark. Each quark can have one of three colors and each quark can have one of three anticolors. Then, in total, we have $3 \times 3 = 9$ color

configurations. Therefore we obtain the $F^2_{9\times 9}$ matrix. In order to reduce the size of matrix, we can take advantage of two operators T_3 and Y. As a result, we only consider three color configurations for the basis states $R\bar{R}$,$G\bar{G}$ and $B\bar{B}$ (where "R" is mnemonic for "red", "B" for "blue" and "G" for "green" single parton color states and the bar indicates an anticolor) since T_3 and Y acting on each of them gives zero. Once we define the basis states we need in color space, we need to diagonalize $F^2_{3\times 3}$.

After diagonalizing F^2, we obtain one color singlet state, which can be expressed as the symmetric superposition

$$\frac{1}{\sqrt{3}}(R\bar{R} + G\bar{G} + B\bar{B}). \tag{3.4}$$

The total wavefunction for a meson in the leading Fock space representation would then consist of a space-spin component for the quark-antiquark system joined with this color space component. More complicated configurations of the meson will be discussed below.

3.1.2 Baryons

Three quarks can also form a color singlet state which is taken to be the leading Fock space configuration of a baryon. Using the same methods, we obtain $F^2_{6\times 6}$ instead of $F^2_{27\times 27}$.

After diagonalizing $F^2_{6\times 6}$, we obtain one color singlet state which is given by.

$$\frac{1}{\sqrt{6}}(RGB - RBG + BRG - BGR + GBR - GRB). \tag{3.5}$$

From the expression above, we can see that the wavefunction is completely antisymmetic in color space.

Here we need to emphasize that the total wavefunction for a system with 3 identical quarks would be composed of a totally symmetric space-spin component joined with this totally antisymmetric color component to produce and overall antisymmetric wavefunction as required by the Pauli exclusion principle.

3.1.3 Glueball

Pure gluon systems can form color singlet states which are called glueballs.

We can find allowed color singlet states of multiple gluons by using F^2. However there are already 64 color configurations for the two-gluon system. In order to reduce the dimensions of the representation of F^2, we can again use the operator T_3 and Y which reduce the original matrix into $F^2_{10\times 10}$ matrix.

After the diagonalization, we found there only exists one color singlet state for two gluons. The color singlet state corresponding to eigenvalue equal to zero is given by

$$\frac{1}{\sqrt{8}}(g^1g^2 + g^2g^1 + g^3g^3 + g^4g^5 + g^5g^4 + g^6g^7 + g^7g^6 + g^8g^8), \tag{3.6}$$

where g^i represents one of eight colors of gluon when i goes from 1 to 8.

We observe that the color wavefunction is completely symmetric if we exchange the first gluon with the second gluon.

Again we need to emphasize that pure gluon systems are bosonic system. Therefore the total wavefunction for the pure gluon system would be composed of a totally symmetric (anti-symmetric) space-spin component joined with this totally symmetric (anti-symmetric) color component to produce and overall symmetric wavefunction for gluon systems as required for boson statistics.

3.1.4 More complicated multiparton hadrons

In the previous sections, we have seen that simple combinations of quarks, antiquarks and gluons can form the color singlet states. Now we need to consider more complicated cases: states with mixtures of quarks, antiquark and gluons. For simplicity, we restrict ourselves to identical quarks and identical antiquarks, each in a distinct space-spin state. The case of identical fermions occupying the same space-spin configuration is a special case with a corresponding reduction in the color-space basis.

At first, we consider the state with one quark, one antiquark and one gluon. Taking advantage of operator T_3 and Y, we have 12 by 12 matrix for operator F^2. After the diagonalization, we found there exists one color singlet state which is given by the following linear combination

of color configurations:

$$\frac{1}{4}(R\bar{R}g^3 - G\bar{G}g^3) + \frac{1}{\sqrt{48}}(R\bar{R}g^8 + G\bar{G}g^8 - 2B\bar{B}g^8)$$
$$+\frac{1}{\sqrt{8}}(R\bar{G}g^2 + R\bar{B}g^5 + G\bar{R}g^1 + G\bar{B}g^7 + B\bar{R}g^4 + B\bar{G}g^6). \tag{3.7}$$

Next we consider a more complicated case: two quarks and two antiquarks. In this case, we obtain two color singlet states. One of these color singlet state has a completely symmetric wavefunction:

$$|sym\rangle = \frac{1}{\sqrt{6}}(RR\bar{R}\bar{R} + GG\bar{G}\bar{G} + BB\bar{B}\bar{B})$$
$$+\frac{1}{\sqrt{24}}(RG\bar{R}\bar{G} + RG\bar{G}\bar{R} + RB\bar{R}\bar{B} + RB\bar{B}\bar{R} + GR\bar{R}\bar{G} + GR\bar{G}\bar{R}$$
$$+GB\bar{G}\bar{B} + GB\bar{B}\bar{G} + BR\bar{R}\bar{B} + BR\bar{B}\bar{R} + BG\bar{G}\bar{B} + BG\bar{B}\bar{G}). \tag{3.8}$$

The other color singlet is completely antisymmetric:

$$|antisym\rangle = \frac{1}{\sqrt{12}}(RG\bar{G}\bar{R} - RG\bar{R}\bar{G} + RB\bar{B}\bar{R} - RB\bar{R}\bar{B} + GR\bar{R}\bar{G} - GR\bar{G}\bar{R}$$
$$+GB\bar{B}\bar{G} - GB\bar{G}\bar{B} + BR\bar{R}\bar{B} - BR\bar{B}\bar{R} + BG\bar{G}\bar{B} - BG\bar{B}\bar{G}). \tag{3.9}$$

With these two color singlet states in hand, we can use them to find the two-meson state as the linear combination of symmetric and antisymmetric color singlet states which is given by

$$\sqrt{\frac{2}{3}}|sym\rangle - \sqrt{\frac{1}{3}}|antisym\rangle$$
$$= \frac{1}{3}(R\bar{R} + G\bar{G} + B\bar{B})(R\bar{R} + G\bar{G} + B\bar{B}). \tag{3.10}$$

Then the other color singlet state which is orthogonal to two-meson state is given by

$$\sqrt{\frac{1}{3}}|sym\rangle + \sqrt{\frac{2}{3}}|antisym\rangle, \tag{3.11}$$

From the example above, we have already seen that within two quark and two antiquark system, we can build up the intrinsic structure of the two-meson state. In the next example, we will see how to construct these kinds of intrinsic structures again.

From the previous section, we know that three quarks can form one color singlet state, the leading configuration for a baryon. One quark and one antiquark can form the leading

configuration for a meson. Therefore within the four quark and one antiquark system, we expect to find the intrinsic color structure of an asymptotic baryon plus meson.

At first, using the methods outlined above, we can obtain a 36 by 36 matrix which represents the operator F^2 in the color basis for these 5 partons. After we diagonalize the matrix, we obtain three color singlet states. The first color singlet state is given by

$$\begin{aligned}
&0.288673(RRGB\bar{R} - RRBG\bar{R} - GGRB\bar{G} + GGBR\bar{G} + BBRG\bar{B} - BBGR\bar{B}) \\
&+0.145076(RBRG\bar{R} - RGRB\bar{R} + GRGB\bar{G} - GBGR\bar{G} - BRBG\bar{B} + BGBR\bar{B}) \\
&+0.143597(RGGB\bar{G} - GRRB\bar{R} - RBBG\bar{B} + GBBR\bar{B} - BGGR\bar{G} + BRRG\bar{R}) \\
&+0.145164(RGBR\bar{R} - RBGR\bar{R} + GBRG\bar{G} - GRBG\bar{G} + BRGB\bar{B} - GBRB\bar{B}) \\
&+0.143509(GRBR\bar{R} - BRGR\bar{R} + BGRG\bar{G} - RGBG\bar{G} + RBGB\bar{B} - GBRB\bar{B}) \\
&+0.000088(GBRR\bar{R} - BGRR\bar{R} + BRGG\bar{G} - RBGG\bar{G} + RGBB\bar{B} - GRBB\bar{B}). \quad (3.12)
\end{aligned}$$

The second color singlet state is given by

$$\begin{aligned}
&0.000062(RRGB\bar{R} - RRBG\bar{R} - GGRB\bar{G} + GGBR\bar{G} + BBRG\bar{B} - BBGR\bar{B}) \\
&+0.149055(RBRG\bar{R} - RGRB\bar{R} + GRGB\bar{G} - GBGR\bar{G} - BRBG\bar{B} + BGBR\bar{B}) \\
&-0.148993(RGGB\bar{G} - GRRB\bar{R} - RBBG\bar{B} + GBBR\bar{B} - BGGR\bar{G} + BRRG\bar{R}) \\
&-0.139543(RGBR\bar{R} - RBGR\bar{R} + GBRG\bar{G} - GRBG\bar{G} + BRGB\bar{B} - GBRB\bar{B}) \\
&+0.139605(GRBR\bar{R} - BRGR\bar{R} + BGRG\bar{G} - RGBG\bar{G} + RBGB\bar{B} - GBRB\bar{B}) \\
&-0.288598(GBRR\bar{R} - BGRR\bar{R} + BRGG\bar{G} - RBGG\bar{G} + RGBB\bar{B} - GRBB\bar{B}). \quad (3.13)
\end{aligned}$$

And the third color singlet state is given by

$$\begin{aligned}
&-0.001110(RRGB\bar{R} - RRBG\bar{R} - GGRB\bar{G} + GGBR\bar{G} + BBRG\bar{B} - BBGR\bar{B}) \\
&+0.200172(RBRG\bar{R} - RGRB\bar{R} + GRGB\bar{G} - GBGR\bar{G} - BRBG\bar{B} + BGBR\bar{B}) \\
&-0.201282(RGGB\bar{G} - GRRB\bar{R} - RBBG\bar{B} + GBBR\bar{B} - BGGR\bar{G} + BRRG\bar{R}) \\
&+0.206854(RGBR\bar{R} - RBGR\bar{R} + GBRG\bar{G} - GRBG\bar{G} + BRGB\bar{B} - GBRB\bar{B}) \\
&-0.207964(GRBR\bar{R} - BRGR\bar{R} + BGRG\bar{G} - RGBG\bar{G} + RBGB\bar{B} - GBRB\bar{B}) \\
&+0.006682(GBRR\bar{R} - BGRR\bar{R} + BRGG\bar{G} - RBGG\bar{G} + RGBB\bar{B} - GRBB\bar{B}). \quad (3.14)
\end{aligned}$$

For the special case where the first two identical quarks occupy the same space-spin configuration, we can modify the approach in color space to respect the Pauli principle in the total basis. To do this, we need to eliminate color configurations in which the first two quarks have the same colors. After we have done this, we have the reduced matrix for F^2 which has dimension 30 by 30. Finally we obtain only two color singlet states corresponding to the requirement that the first two quarks can not have the same color. We list out these two color singlet states.

The first one is given by

$$\begin{aligned}
&0.015734(-RGRB\bar{R} - RGGB\bar{G} - GBGR\bar{G} - GBBR\bar{B} - BRRG\bar{R} - BRBG\bar{B} \\
&\quad +RBRG\bar{R} + RBBG\bar{B} + GRRB\bar{R} + GRGB\bar{G} + BGGR\bar{G} + BGBR\bar{B}) \\
&+0.229990(-RGBR\bar{R} - RGBG\bar{G} - GBRG\bar{G} - GBRB\bar{B} - BRGR\bar{R} - BRGB\bar{B} \\
&\quad +RBGR\bar{R} + RBGB\bar{B} + GRBR\bar{R} + GRBG\bar{G} + BGRG\bar{G} + BGRB\bar{B}) \\
&+0.245724(-RGBB\bar{B} + RBGG\bar{G} + GRBB\bar{B} - GBRR\bar{R} - BRGG\bar{G} + BGRR\bar{R}). \quad (3.15)
\end{aligned}$$

The second one is given by

$$\begin{aligned}
&0.249504(RGRB\bar{R} + RGGB\bar{G} + GBGR\bar{G} + GBBR\bar{B} + BRRG\bar{R} + BRBG\bar{B} \\
&\quad -RBRG\bar{R} - RBBG\bar{B} - GRRB\bar{R} - GRGB\bar{G} - BGGR\bar{G} - BGBR\bar{B}) \\
&+0.098002(-RGBR\bar{R} - RGBG\bar{G} - GBRG\bar{G} - GBRB\bar{B} - BRGR\bar{R} - BRGB\bar{B} \\
&\quad +RBGR\bar{R} + RBGB\bar{B} + GRBR\bar{R} + GRBG\bar{G} + BGRG\bar{G} + BGRB\bar{B}) \\
&+0.151502(RGBB\bar{B} - RBGG\bar{G} - GRBB\bar{B} + GBRR\bar{R} + BRGG\bar{G} - BGRR\bar{R}). \quad (3.16)
\end{aligned}$$

We can change these two singlet states into the new forms. The first singlet state is

$$\begin{aligned}
&0.015734(-RGRB\bar{R} - RGGB\bar{G} - GBGR\bar{G} - GBBR\bar{B} - BRRG\bar{R} - BRBG\bar{B} \\
&\quad +RBRG\bar{R} + RBBG\bar{B} + GRRB\bar{R} + GRGB\bar{G} + BGGR\bar{G} + BGBR\bar{B} \\
&\quad -RGBB\bar{B} + RBGG\bar{G} + GRBB\bar{B} - GBRR\bar{R} - BRGG\bar{G} + BGRR\bar{R}) \\
&+0.229990(-RGBR\bar{R} - RGBG\bar{G} - GBRG\bar{G} - GBRB\bar{B} - BRGR\bar{R} - BRGB\bar{B} \\
&\quad +RBGR\bar{R} + RBGB\bar{B} + GRBR\bar{R} + GRBG\bar{G} + BGRG\bar{G} + BGRB\bar{B}
\end{aligned}$$

$$
\begin{aligned}
& -RGBB\bar{B} + RBGG\bar{G} + GRBB\bar{B} - GBRR\bar{R} - BRGG\bar{G} + BGRR\bar{R}) \\
= \quad & 0.015734(-RG(R\bar{R} + G\bar{G} + B\bar{B})B + RB(R\bar{R} + G\bar{G} + B\bar{B})G - BR(R\bar{R} + G\bar{G} + B\bar{B})G \\
& +BG(R\bar{R} + G\bar{G} + B\bar{B})R - GB(R\bar{R} + G\bar{G} + B\bar{B})R + GR(R\bar{R} + G\bar{G} + B\bar{B})B) \\
& +0.229990(-RGB + RBG - BRG + BGR - GBR + GRB)(R\bar{R} + G\bar{G} + B\bar{B}). \qquad (3.17)
\end{aligned}
$$

Using the same method, we can get a very similar structure for the second singlet state. From these two states, we note that we can construct two color singlet states which then simulate an interesting intrinsic structure. The first one appears as the color product space of the baryon and the meson

$$(-RGB + RBG - BRG + BGR - GBR + GRB)(R\bar{R} + G\bar{G} + B\bar{B}). \qquad (3.18)$$

The second one appears as an intrinsic state of these 5 partons that does not separate into the asymptotic state of a meson and a baryon

$$
\begin{aligned}
& (-RG(R\bar{R} + G\bar{G} + B\bar{B})B + RB(R\bar{R} + G\bar{G} + B\bar{B})G - BR(R\bar{R} + G\bar{G} + B\bar{B})G \\
& +BG(R\bar{R} + G\bar{G} + B\bar{B})R - GB(R\bar{R} + G\bar{G} + B\bar{B})R + GR(R\bar{R} + G\bar{G} + B\bar{B})B). \qquad (3.19)
\end{aligned}
$$

The above construction was carried out in order to illustrate the challenges of discerning substructures within complicated multi-parton color space states. We have found no general method that is guaranteed to reveal substructures of multi-parton color space states.

Next, we consider the case with three quarks and three antiquarks.

Using the operator F^2, we have the conclusion that there exists six color singlet states which have the required zero eigenvalues.

And we have only one color singlet state with completely symmetric wavefunction which is given by

$$
\begin{aligned}
& \frac{1}{\sqrt{10}}(RRR\bar{R}\bar{R}\bar{R} + GGG\bar{G}\bar{G}\bar{G} + BBB\bar{B}\bar{B}\bar{B}) \\
& +\frac{1}{\sqrt{90}}(RRG\bar{R}\bar{R}\bar{G} + c.s.p) \\
& +\frac{1}{\sqrt{90}}(RRB\bar{R}\bar{R}\bar{B} + c.s.p) \\
& +\frac{1}{\sqrt{90}}(GGR\bar{G}\bar{G}\bar{R} + c.s.p)
\end{aligned}
$$

$$+\frac{1}{\sqrt{90}}(BBR\bar{B}\bar{B}\bar{R}+c.s.p)$$
$$+\frac{1}{\sqrt{90}}(GGB\bar{G}\bar{G}\bar{B}+c.s.p)$$
$$+\frac{1}{\sqrt{90}}(BBG\bar{B}\bar{B}\bar{G}+c.s.p)$$
$$+\frac{1}{\sqrt{360}}(RGB\bar{R}\bar{G}\bar{B}+c.s.p), \tag{3.20}$$

where c.s.p represents the complete symmetric partners.

The other five color singlet states are either antisymmetic or possess mixed symmetry.

3.1.5 Summary of multiparton hadrons

In this section, we give a summary of multiparton hadrons. Some of the results we obtained are displayed in Fig. 3.1. In Fig. 3.1, the upper curves are counts of all color configurations with zero color projection after we employ the operator constraints provided by T_3 and Y. The lower curves are counts of global color singlet states resulting from diagonalization for the specified number of quarks and gluons.

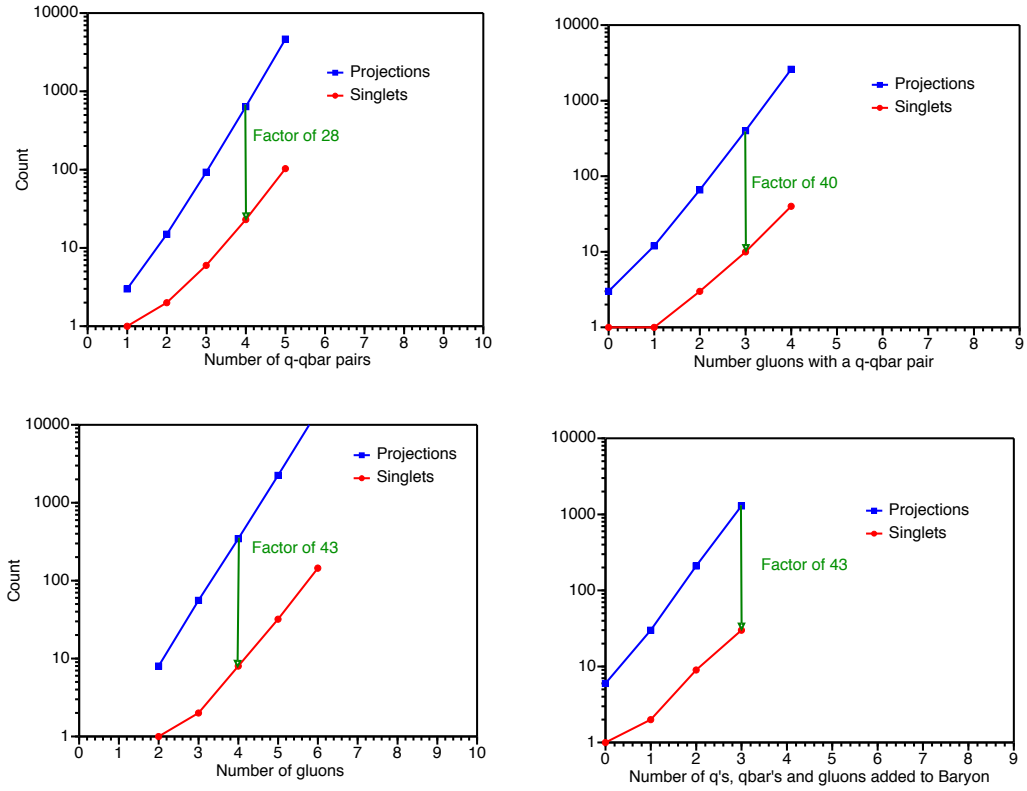

Figure 3.1 Number of color space states that apply to each space-spin configuration of selected multi-parton states for two methods of enumerating the color basis states. The upper curves are counts of all color configurations with zero color projection. The lower curves are counts of global color singlets.

The more complete results are summarized in Tables listed as follows.

Number of gluons	Color singlet projection	Number of color singlet states
2	10	1
3	56	2
4	346	8
5	2252	32
6	15184	145

Table 3.1 Number of color singlet states and color singlet projection for given number of gluons.

Number of quarks	Color singlet projection	Number of color singlet states
3	6	1
6	90	5
9	1680	42

Table 3.2 Number of color singlet states and color singlet projection for given number of quarks.

(Quarks, antiquarks)	Color singlet projection	Number of color singlet states
(1,1)	3	1
(2,2)	15	2
(3,3)	93	6
(4,4)	639	23
(5,5)	4653	103
(1,4)	36	3
(1,7)	630	21
(5,2)	240	11

Table 3.3 Number of color singlet states and color singlet projection for given number of quarks and antiquarks.

(Quarks, gluons)	Color singlet projection	Number of color singlet states
(3,1)	30	2
(3,2)	174	6
(3,3)	1092	22
(3,4)	7188	92
(6,1)	540	16
(6,2)	3450	61

Table 3.4 Number of color singlet states and color singlet projection for given number of quarks and gluons.

(Quarks, antiquarks,gluons)	Color singlet projection	Number of color singlet states
(1,1,1)	12	1
(1,1,2)	66	3
(1,1,3)	402	10
(1,1,4)	2598	40
(2,2,1)	78	4
(2,2,2)	468	13
(2,2,3)	3000	50
(3,3,1)	546	17
(3,3,2)	3468	63

Table 3.5 Number of color singlet states and color singlet projection for given number of quarks and antiquarks and gluons.

3.1.6 Global symmetry of multiparton hadrons

In the previous sections, we mentioned that to obtain the multiparton hadrons, systems of mesons and baryons that can involve dynamic gluon configurations, we need to construct the generic algebra in color space such that we can obtain singlet states of particles constructed from any arbitrary number of partons in principle. However, in the previous section we restricted the discussion to the situation where identical fermions occupy distinct space-spin single-particle modes such that in color space, identical fermions are able to occupy the same

state in color. The case where we allow multiple space-spin occupancies by identical fermions leads to color space restrictions. Therefore we need to consider the situation where identical fermions occupy the same space-spin single-particle mode and consequently, they need to have the different colors in color space. In this section, we try to show some results when we put the restrictions on color spaces.

At first, we consider the case where we have multiquarks and antiquarks. We require that the first two quarks must have different colors if they are in the same space-spin single-particle mode. The results are given in Table 3.6.

(Quarks, antiquarks)	Color singlet projection	Number of color singlet states
(2,2)	12	1
(3,3)	72	3
(4,4)	480	11
(5,5)	3420	47
(1,4)	30	2
(1,7)	480	11
(5,2)	186	6

Table 3.6 Number of color singlet states and color singlet projection for given number of quarks and antiquarks when we require that the first two quarks have different colors.

We can see that in Table 3.6, the color singlet states and color singlet projection are reduced compared with the same configurations in Table 3.3.

We can also require that the first three quarks have different colors if they are in the same space-spin single-particle mode. The results are given in Table 3.7.

Since the antiquarks are also identical particles, we have the situation where we require the first two antiquarks in the different colors except that the first two quarks have different colors. If we put that restrictions in the color space, we have the results which are summarized in the Table 3.8.

(Quarks, antiquarks)	Color singlet projection	Number of color singlet states
(3,3)	36	1
(4,4)	216	3
(5,5)	1440	11
(1,4)	18	1
(1,7)	216	3
(5,2)	90	2

Table 3.7 Number of color singlet states and color singlet projection for given number of quarks and antiquarks when we require that the first three quarks have different colors.

(Quarks, antiquarks)	Color singlet projection	Number of color singlet states
(2,2)	12	1
(3,3)	60	2
(4,4)	216	3
(5,5)	2556	23

Table 3.8 Number of color singlet states and color singlet projection for given number of quarks and antiquarks when we require that the first two quarks and antiquarks have different colors.

CHAPTER 4. CAVITY MODE PHYSICS

Having addressed the background of QCD and many of the technical details for solving Hamiltonian light front field theory, we now turn our attention to a specific illustrative application of a light front cavity mode field theory. It is worth recounting at the outset, some of the overall motivations for the approach that we will follow and the links to related efforts in nuclear many-body theory.

4.1 Introduction

Non-perturbative Hamiltonian light-front quantum field theory presents opportunities and challenges that bridge particle physics and nuclear physics. Major goals include predicting both the masses and transitions rates of the hadrons and their structures as seen in high-momentum transfer experiments. Current focii of intense experimental and theoretical research that could benefit from insights derived within this Hamiltonian approach include the spin structure of the proton, the neutron electromagnetic form factor, the generalized parton distributions of the baryons, etc.

Hamiltonian light-front field theory in a discretized momentum basis [15] and in transverse lattice approaches [16, 17, 18] have shown significant promise. We present here a basis-function approach that exploits recent advances in solving the non-relativistic strongly interacting nuclear many-body problem [19, 20]. We note that both light-front field theory and nuclear many-body theory face common issues within the Hamiltonian approach - i.e. how to (1) define the Hamiltonian; (2) renormalize to a finite space; (3) solve for non-perturbative observables while preserving as many symmetries as possible; and, (4) take the continuum limit. In spite of the technical hurdles, Ken Wilson has assessed the advantages of adopting advances

in quantum many-body theory and has long advocated adoption of basis function methods as an alternative to the lattice gauge approach [21].

There are three main advantages of Hamiltonian light-front quantum field theory motivating our efforts to overcome the technical hurdles. First, one evaluates experimental observables that are non-perturbative and relativistically invariant quantities such as masses, form factors, structure functions, etc. Second, one evaluates these quantities in Minkowski space and, third, there is no fermion doubling problem.

We begin this chapter with a brief overview of recent advances in solving light nuclei with realistic nucleon-nucleon (NN) and three-nucleon (NNN) interactions using *ab initio* no-core methods in a basis function representation. Then, we introduce our basis function approach to light-front QCD within the light-front gauge. Renormalization/regularization issues are also addressed. We present illustrative features of our approach with the example of cavity-mode QED and sketch its extension to cavity-mode QCD.

The present chapter is an expanded version of a recent paper where we provided an initial introduction to our approach [22] and itself is the foundation for a recently submitted paper [23].

4.2 Choice of Representation for Light Front Hamiltonians

It has long been known that light-front Hamiltonian quantum field theory has similarities with non-relativistic quantum many-body theory. We further exploit this connection, in what we will term a "Basis Light Front Quantized (BLFQ)" approach, by adopting a light-front single-particle basis space consisting of the 2-D harmonic oscillator for the transverse modes (radial coordinate ρ and polar angle ϕ) and a discretized momentum space basis for the longitudinal modes. Adoption of this basis is also consistent with recent developments in AdS/CFT correspondence with QCD [28, 29, 30, 31, 32]. In the present application to the non-interacting problem, we will adopt periodic boundary conditions (PBC) for the longitudinal modes and we omit the zero mode. For our light-front coordinates, we define, in concert with previous chapters, $x^{\pm} = x^0 \pm x^3$, $x^{\perp} = (x^1, x^2)$ and the coordinate pair (ρ, ϕ) are the usual cylin-

drical coordinates in (x^1, x^2). The variable x^+ is light-front time and x^- is the longitudinal coordinate. We adopt $x^+ = 0$, the "null plane", for our quantization surface.

The 2-D oscillator states are characterized by their principal quantum number n, orbital quantum number m and harmonic oscillator energy Ω. It is also convenient to interpret the 2-D oscillator as a function of the dimensionless radial variable $\sqrt{M_0\Omega}\rho$ where M_0 has units of mass and ρ is the conventional radial variable in units of length. Thus, the length scale for transverse modes is set by the chosen value of $\sqrt{M_0\Omega}$. The details about 2-D Harmonic oscillator wavefunctions are discussed in Appendix B.

The properly orthonormalized wavefunctions, $\Phi_{n,m}(\rho,\phi) = \langle\rho\phi|nm\rangle \ = f_{n,m}(\rho)\chi_m(\phi)$, are given in terms of the Generalized Laguerre Polynomials, $L_n^{|m|}(M_0\,\Omega\,\rho^2)$, by

$$f_{n,m}(\rho) \ = \ \sqrt{2\,M_0\,\Omega}\,\sqrt{\frac{n!}{(n+|m|)!}}\,\mathrm{e}^{-M_0\,\Omega\,\rho^2/2}\,\left(\sqrt{M_0\,\Omega}\,\rho\right)^{|m|}\,L_n^{|m|}(M_0\,\Omega\,\rho^2) \qquad (4.1)$$

$$\chi_m(\phi) \ = \ \frac{1}{\sqrt{2\pi}}\,\mathrm{e}^{i\,m\,\phi} \qquad (4.2)$$

with eigenvalues $E_{n,m} = (2n + |m| + 1)\Omega$. The orthonormalization is fixed by

$$\langle nm|n'm'\rangle \ = \ \int_0^\infty \int_0^{2\pi} \rho\,d\rho\,d\phi\;\Phi_{n,m}(\rho,\phi)^*\;\Phi_{n',m'}(\rho,\phi) \ = \ \delta_{n,n'}\;\delta_{m,m'} \qquad (4.3)$$

which allows for an arbitrary phase factor $\mathrm{e}^{i\alpha}$ that we have taken to be unity. One of the significant advantages of the 2-D oscillator basis is the relative ease for transforming results between coordinate space and momentum space. That is, the Fourier transformed wavefunctions have the same analytic structure in both coordinate and momentum space, a feature reminiscent of a plane-wave basis.

In order to gain an impression of the transverse modes in our light-front basis, we present in Figs. 4.1, 4.2, 4.3, 4.4 and 4.5 snapshots of selected low-lying modes. As one increases the orbital quantum number m, pairs of maxima and minima populate the angular dependence of the basis function. Also, as one increases the principal quantum number n, additional radial nodes appear as evident in the progression from Fig. 4.1 to Fig. 4.5.

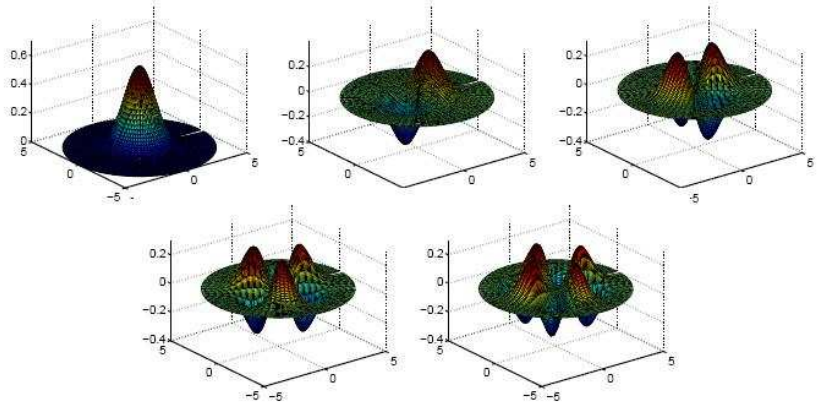

Figure 4.1 Modes for $n = 0$ of the 2-D harmonic oscillator. The orbital quantum number m progresses across the rows by integer steps from 0 in the upper left to 4 in the lower right.

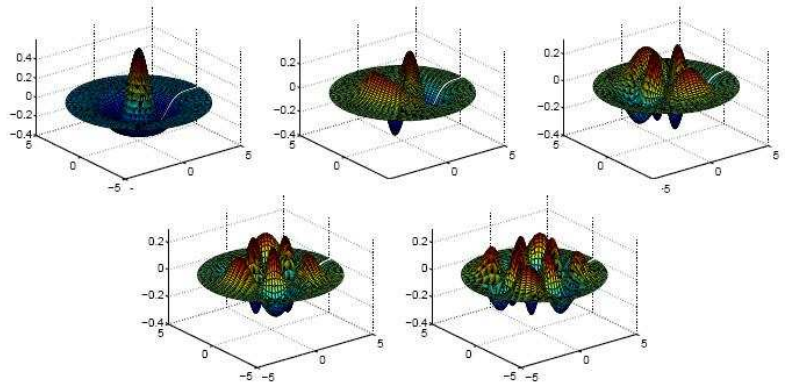

Figure 4.2 Modes for $n = 1$ of the 2-D harmonic oscillator. The orbital quantum number m progresses across the rows by integer steps from 0 in the upper left to 4 in the lower right.

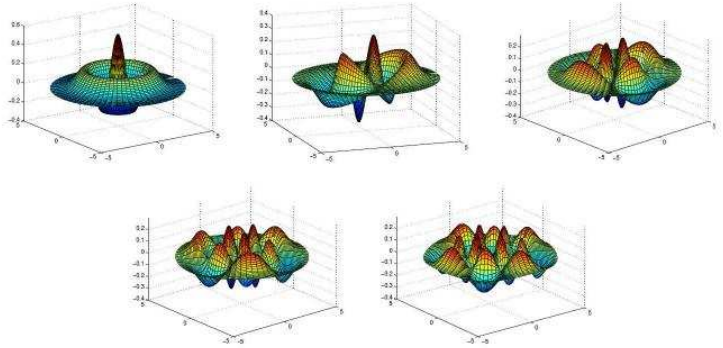

Figure 4.3 Modes for $n = 2$ of the 2-D harmonic oscillator. The orbital quantum number m progresses across the rows by integer steps from 0 in the upper left to 4 in the lower right.

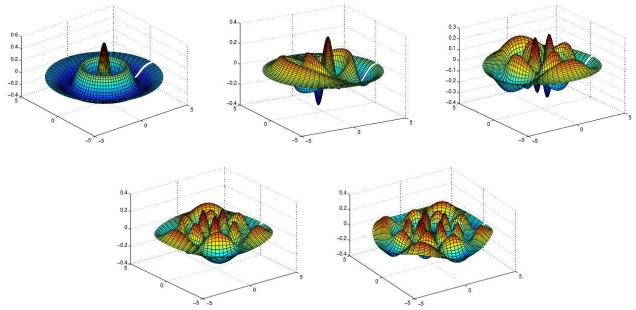

Figure 4.4 Modes for $n = 3$ of the 2-D harmonic oscillator. The orbital quantum number m progresses across the rows by integer steps from 0 in the upper left to 4 in the lower right.

To provide a perspective on the full 3-D basis, we introduce longitudinal modes ψ_j defined on $-L \leq x^- \leq L$ with both periodic boundary conditions (PBC) and antiperiodic boundary conditions (APBC). We also introduce a purely real form to be used in Fig. 4.6 and Fig. 4.7.

$$\psi_k(x^-) = \frac{1}{\sqrt{2L}} \, \mathrm{e}^{i \frac{\pi}{L} k \, x^-} \tag{4.4}$$

$$\psi_k(x^-) = \frac{1}{\sqrt{\pi L}} \sin \frac{\pi}{L} k \, x^- \tag{4.5}$$

where $k = 1, 2, 3, ...$ for PBC (neglecting the zero mode) and $k = \frac{1}{2}, \frac{3}{2}, \frac{5}{2}, ...$ in Eqn.(4.4) for APBC. Similarly, $k = 1, 2, 3$ in Eqn.(4.5) for reflection antisymmetric amplitudes with box boundary conditions (amplitude vanishes at $x^- = \pm L$). The full 3-D single particle basis state is defined by the product form

$$\Psi_{k,n,m}(x^-, \rho, \phi) = \psi_k(x^-) \Phi_{n,m}(\rho, \phi). \tag{4.6}$$

Then the Fock space expansions for fermion field are

$$\eta(x^-, \rho, \phi) = \sum_{k,n,m} \left(b(k,n,m) \Psi_{k,n,m}(x^-, \rho, \phi) + d^\dagger(k,n,m) \Psi^\star_{k,n,m}(x^-, \rho, \phi) \right) \tag{4.7}$$

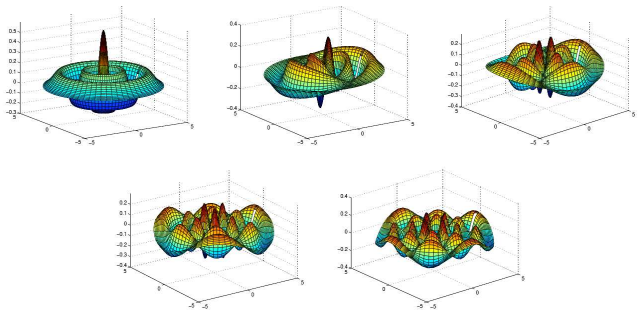

Figure 4.5 Modes for $n = 4$ of the 2-D harmonic oscillator. The orbital quantum number m progresses across the rows by integer steps from 0 in the upper left to 4 in the lower right.

The commutation relations are

$$\begin{aligned} \{b(k_1, n_1, m_1), b^\dagger(k_2, n_2, m_2)\} &= \delta_{k_1,k_2}\delta_{n_1,n_2}\delta_{m_1,m_2} \\ \{d(k_1, n_1, m_1), d^\dagger(k_2, n_2, m_2)\} &= \delta_{k_1,k_2}\delta_{n_1,n_2}\delta_{m_1,m_2} \end{aligned} \tag{4.8}$$

For a first illustration, we select a transverse mode with $n = 1, m = 0$ joined together with the $k = \frac{1}{2}$ longitudinal APBC mode of Eqn. (4.4) and display slices of the real part of this 3-D basis function at selected longitudinal coordinates, x^- in Fig. 4.6. For comparison, we present a second example with Eqn. (4.5) for the longitudinal mode in Fig. 4.7. Our purpose in presenting both Figs. 4.6 and 4.7 is to suggest the richness, flexibility and economy of texture available for solutions in a basis function approach. Note that the choice of basis functions is rather arbitrary, including which boundary conditions are imposed, except for the standard conditions of orthonormality and completeness within the selected symmetries.

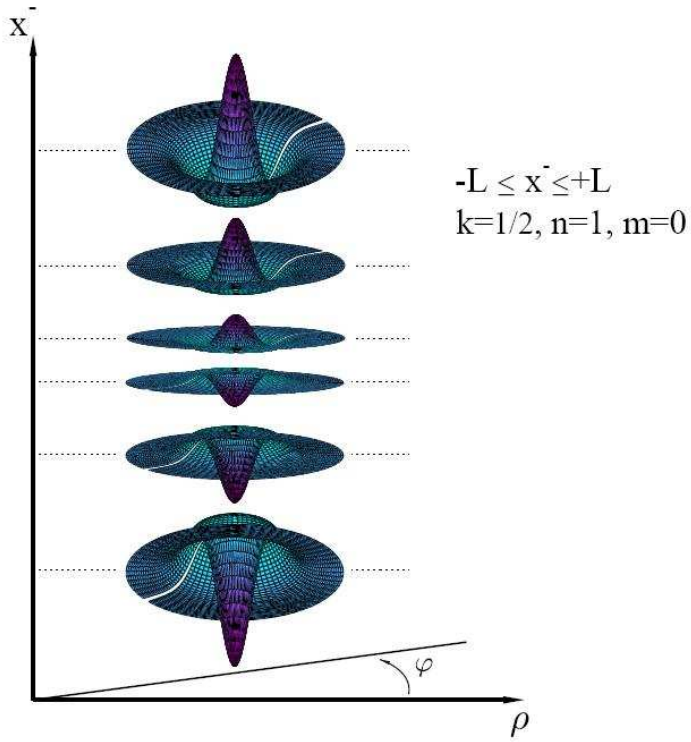

Figure 4.6 Transverse sections of the real part of a 3-D basis function involving a 2-D harmonic oscillator and a longitudinal mode of Eqn. (4.4) with antiperiodic boundary conditions (APBC). The quantum numbers for this basis function are given in the isucaption. The basis function is shown for the full range $-L \leq x^- \leq L$.

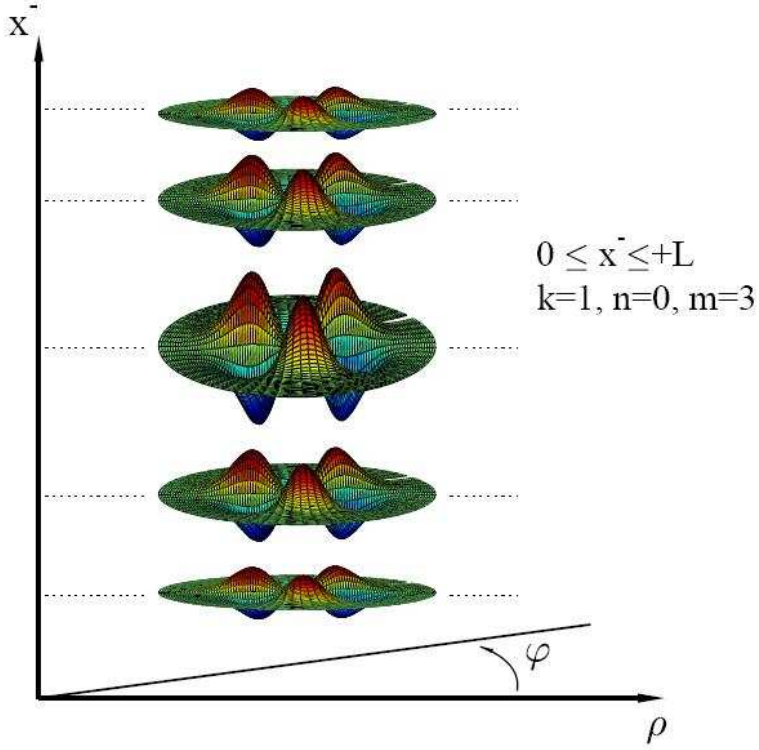

Figure 4.7 Transverse sections of a 3-D basis function involving a 2-D harmonic oscillator and a longitudinal mode of Eqn. (4.5) with box boundary conditions (wavefunction vanishes at ±L). The quantum numbers for this basis function are given in the isucaption. The basis function is shown for positive values of x^- and is antisymmetric with respect to $x^- = 0$

Although our choice of basis functions is not dictated by theory, it is buttressed by the phenomenological success of the "soft-wall" AdS/QCD model[28, 29] which uses a harmonic oscillator potential in the fifth dimension of Anti-de Sitter space to simulate color confinement. As shown in ref. [30] one can use "light-front holography"[31] to transform the bound state equations for the wavefunction in AdS space[32] to a corresponding bound-state equation in physical space at fixed light-front time τ. The resulting light-front equation is similar in form to the Schrödinger radial wave equation at fixed t which describes the quantum-mechanical structure of atomic systems. However, the formalism at fixed light-front time is relativistic and frame independent. Thus, for the specific example of a $q\bar{q}$ pair, one obtains a relativistic

wave equation applicable to hadron physics, where the light-front coordinate $\zeta = b_\perp \sqrt{x(1-x)}$ plays the role of the radial variable r of the nonrelativistic theory. Here, x is the light-front momentum fraction of the quark and $b_\perp$ is the magnitude of the transverse relative separation coordinate. In this example, the meson eigenvalue equation is[30]

$$\left[-\frac{d^2}{d\zeta^2} - \frac{1-4L^2}{4\zeta^2} + U(\zeta)\right]\phi(\zeta) = M^2\phi(\zeta), \tag{4.9}$$

where the complexity of the QCD interactions among constituents is summed up in the addition of the effective potential $U(\zeta)$, which is then modeled to enforce confinement. The potential in the soft wall model is $U(\zeta) = \kappa^4\zeta^2 + 2\kappa^2(J-1)$ where J is the total angular momentum of the hadron. Using the substitutions $\phi(\zeta) = \zeta^{1/2}R(\zeta)$, $\kappa\zeta = \sqrt{M_0\Omega}\rho$ and $L = |m|$, we arrive at the transverse 2-D harmonic oscillator wave equation whose solution is given in Eqn. (B.25).

There is one additional distinction between our choice of transverse basis functions and the solutions of the AdS/QCD model: we adopt single-parton coordinates as the basis function arguments while AdS/QCD adopts a relative coordinate between the constituents. Our selection is natural for the applications within an external cavity that we present here and is most convenient for enforcing the boson and fermion statistics when dealing with arbitrary many partons. In future work without the external cavity, we may invoke a Lagrange multiplier method, analogous to the method in the NCSM and NCFC approaches [19, 20], to separate the relative motion from the total system's motion in the transverse direction.

The solutions of the light-front equation (4.9) determine the masses of the hadrons, given the total internal spin S, the orbital angular momenta L of the constituents, and the index n, the number of nodes of the wavefunction in ζ. For example, if the total quark spin S is zero, the meson bound state spectrum follows the quadratic form $M^2 = 4\kappa^2(n+L)$. Thus the internal orbital angular momentum L and its effect on quark kinetic energy play an explicit role. The corresponding wavefunctions of the mesonic eigensolutions describe the probability distribution of the $q\bar{q}$ constituents for the different orbital and radial states. The separation of the constituent quark and antiquark in AdS space get larger as the orbital angular momentum increases. The pion with $n = 0$ and $L = 0$ is massless for zero quark mass, in agreement with general arguments based on chiral symmetry. If the total spin of the constituents is $S = 1$, the

corresponding mass formula for the orbital and radial spectrum of the ρ and ω vector mesons is $M^2 = 4\kappa^2(n + L + 1/2)$. The states are aligned along linear Regge trajectories and agree well with experiment. The resulting light-front wavefunctions also give a good account of the hadron form factors.

The AdS/QCD model, together with light-front holography, provides a semiclassical first approximation to strongly coupled QCD. The BLFQ approach in this paper provides a natural extension of the AdS/QCD light-front wavefunctions to multiquark and multi-gluonic Fock states, thus allowing for particle creation and absorption. By setting up and diagonalizing the light-front QCD Hamiltonian on this basis, we incorporate higher order corrections corresponding to the full QCD theory, and we hope to gain insights into the success of the AdS/QCD model.

4.3 Cavity mode light-front field theory without interactions

For a first application of the BLFQ approach, we consider a non-interacting QED system confined to a transverse harmonic trap or cavity. For simplicity, we take the spin 1/2 leptons as massless. The basis functions are matched to the trap so we implement a transverse 2-D harmonic oscillator basis with length scale fixed by the trap and finite modes in the longitudinal direction with APBC. Since we are ultimately interested in the self-bound states of the system, we anticipate adoption of the NCSM method for factorizing the eigensolutions into simple products of intrinsic and total momentum solutions in the transverse direction [19]. That is, with a suitable transverse momentum constraint such as a large positive Lagrange multiplier times the 2-D harmonic oscillator Hamiltonian acting on the total transverse coordinates, the low-lying physical solutions will all have the same expectation value of total transverse momentum squared. Therefore, following Ref. [15] we introduce the total invariant mass-squared M^2 for these low-lying physical states in terms of a Hamiltonian H times a dimensionless integer for the total light front momentum K

$$M^2 + P_\perp P_\perp \to M^2 + const = P^+P^- = KH \tag{4.10}$$

where we absorb the constant into M^2. The Hamiltonian H for this system is defined by the sum of the occupied modes i in each many-parton state with the scale set by the combined constant $\Lambda^2 = 2M_0\Omega$:

$$H = 2M_0 P_c^- = \frac{2M_0\Omega}{K} \sum_i \frac{2n_i + |m_i| + 1}{x_i}. \tag{4.11}$$

We adopt symmetry constraints and two cutoffs for our many-parton states. For symmetries, we fix the total charge Z, the total azimuthal quantum number M_t, and the total spin projection S along the x^- direction. For cutoffs, we select the total light-front momentum, K, and the maximum total quanta allowed in the transverse mode of each many-parton state, N_{max}. For the longitudinal modes, we select those with PBC from Eqn.(4.4). The chosen symmetries and cutoffs are expressed in terms of sums over the quantum numbers of the single-parton degrees of freedom contained in each many-parton state of the system in the following way:

$$\sum_i q_i = Z \tag{4.12}$$

$$\sum_i m_i = M_t \tag{4.13}$$

$$\sum_i s_i = S \tag{4.14}$$

$$\sum_i x_i = 1 = \frac{1}{K} \sum_i k_i \tag{4.15}$$

$$\sum_i 2n_i + |m_i| + 1 \leq N_{max} \tag{4.16}$$

where, for example, k_i is the integer that defines the PBC longitudinal modes of Eqn. (4.4) for the i^{th} parton. The range of the number of fermion-antifermion pairs and bosons is limited by the cutoffs in the modes (K and N_{max}). Since each parton carries at least one unit of longitudinal momentum, the basis is limited to K partons. Furthermore, since each parton carries at least one oscillator quanta for transverse motion, the basis is also limited to N_{max} partons. Thus the combined limit on the number of partons is $\min(K, N_{max})$. In principle, one may elect to further truncate the many-parton basis by limiting the number of fermion-antifermion pairs and/or the number of bosons but we have not elected to do so here.

We may refer to the quantity K as the inverse longitudinal harmonic resolution. We reason that as we increase K, higher longitudinal momenta states become available to the partons, thus allowing finer detail in the features of the longitudinal coordinate structure to emerge.

In a fully interacting application, the actual choice of symmetry constraints will depend on those dictated by the Hamiltonian. For example, with QCD we would add color and flavor attributes to the single particle states and apply additional symmetries such as requiring all many-parton states to be global color singlets as discussed in previous chapters. Another example is the choice to conserve total $M_t + S$ rather than conserving each separately as chosen here. It is straightforward, but sometimes computationally challenging, to modify the symmetries in a basis function approach such as we adopt here. However, in order to approach the continuum limit (all cutoffs are removed) as closely as possible with limited computational resources, one works to implement as many of the known symmetries as possible.

4.3.1 Basis space dimensions

For our defined non-interacting cavity mode problem, we now illustrate the exponential rise in basis-space dimensions with increasing N_{max} at fixed K, with increasing K at fixed N_{max} and with simultaneous increase in both cutoffs. The first two situations involve a parton number cutoff defined by K and N_{max} respectively. Only the case with simultaneous increase in cutoffs keeps the problem physically interesting at higher excitations since this is the only case with unlimited number of partons as both cutoffs go to infinity.

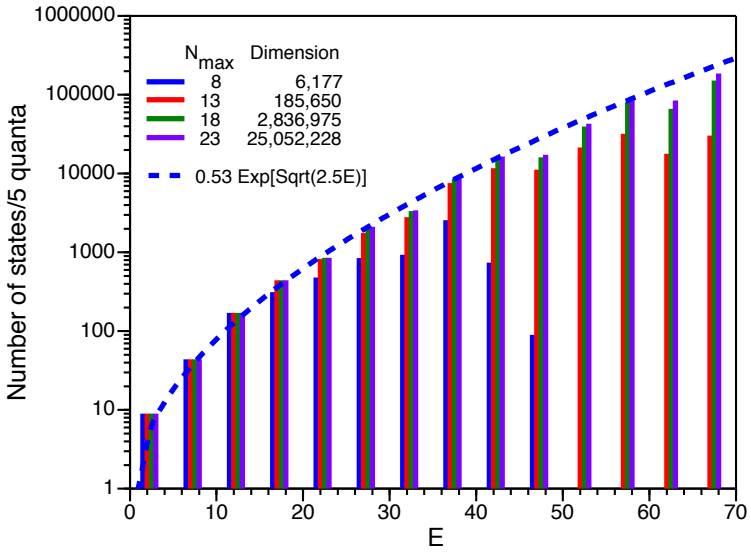

Figure 4.8 State density as a function of dimensionless state energy E from BLFQ for non-interacting QED in a trap with no net charge and for a selection of N_{max} values at fixed $K = 6$. The dimensions of the resulting matrices are presented in the legend. The states are binned in groups of 5 units of energy (quanta) where each parton carries energy equal to its 2-D oscillator quanta $(2n_i + |m_i| + 1)$ divided by its light-front momentum fraction $(x_i = k_i/K)$. The dashed line traces an exponential in the square root of energy that reasonably approximates the histogram at larger N_{max} values.

In Fig. 4.8 we present the state density in BLFQ for massless QED in the zero coupling limit for the case with no net charge $Z = 0$, i.e. for zero lepton number. Thus the cavity is populated by many-parton states consisting of fermion-antifermion pairs and photons. The chosen symmetries are $M = 0$ and $S = 0$. We show results for $K = 6$ at various values of N_{max} spanning a range ($N_{max} = 8 - 23$) . The states are grouped to form a histogram according to their energy calculated from the chosen Hamiltonian in Eqn. (4.11) where we omit the constant preceding the summation for simplicity. Similarly, in Fig. 4.9 we present the state densities for $Z = 3$, $M_t = 0$ and $S = 1/2$ at the same selected values of N_{max}.

Both Figs. 4.8 and 4.9 demonstrate the saturation of low-lying modes with increasing N_{max}.

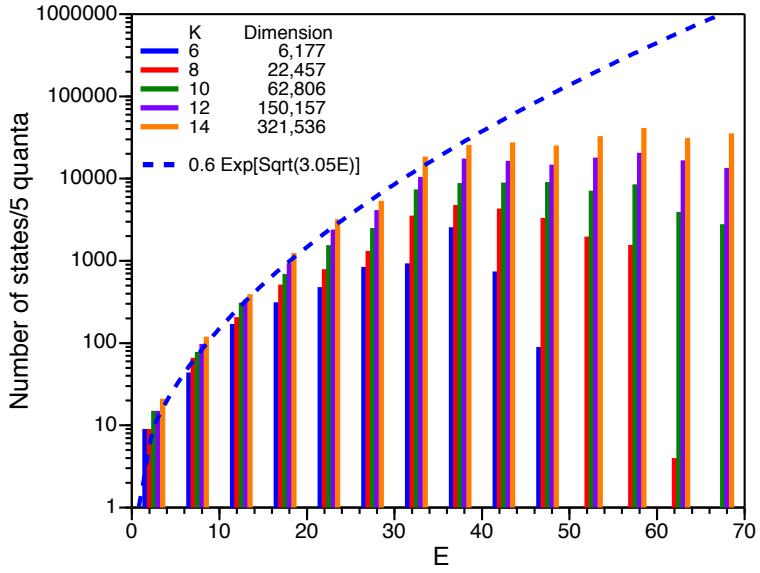

Figure 4.9 State density as a function of dimensionless state energy E from BLFQ for non-interacting QED in a trap with net charge of 3 and for a selection of N_{max} values at fixed $K = 6$. The dimensions of the resulting matrices are presented in the legend. The states are binned in groups of 5 units of energy (quanta) where each parton carries energy equal to its 2-D oscillator quanta $(2n_i + |m_i| + 1)$ divided by its light-front momentum fraction $(x_i = k_i/K)$. The dashed line traces an exponential in the square root of energy that reasonably approximates the histogram at larger N_{max} values.

That is, in each case, one may observe an excitation energy at which the state density reaches a value that no longer changes with increasing N_{max}. The energy at which this saturation occurs, increases with N_{max}. We show only the lower sections of some of the state density distributions but it is clear that all distributions must fall off at sufficiently high energy for fixed N_{max} and K.

In Fig. 4.10 we present the state density in BLFQ for QED in the zero coupling limit again for the case with no net charge $Z = 0$ but with increasing K at fixed $N_{max} = 8$. In this case the many-parton states at low energy continue to increase in number with increasing K. This is understandable from the definition of the Hamiltonian in Eqn. (4.11). In particular,

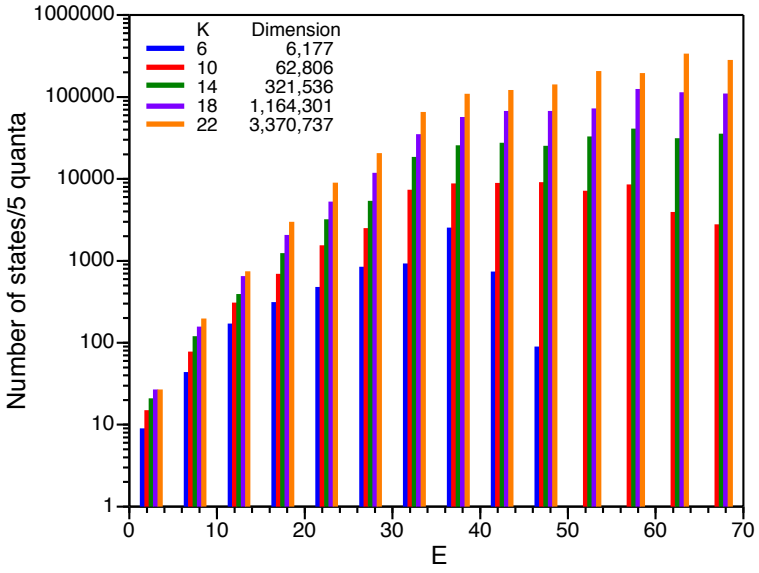

Figure 4.10 State density as a function of dimensionless state energy E from BLFQ for non-interacting QED in a trap with no net charge and for a selection of K values at fixed $N_{max} = 8$. The dimensions of the resulting matrices are presented in the legend. The states are binned in groups of 5 units of energy (quanta) where each parton carries energy equal to its 2-D oscillator quanta $(2n_i + |m_i| + 1)$ divided by its light-front momentum fraction $(x_i = k_i/K)$.

a typical fermion-antifermion state with each parton's light-front momentum fraction close to $x_i = \frac{1}{2}$ achieves a low energy. Correspondingly, as one increases K, the population of states at low E grows since there are more pairs of values of x_i near $\frac{1}{2}$ to employ for minimizing the energy. This reasoning easily extends to states with increasing numbers of partons so the net result is an increasing level density with increasing K at fixed low E and fixed N_{max}.

For the final example of state densities, we consider the case where both K and N_{max} increase simultaneously. For simplicity, we remain with the $Z = 0$ sector and take $K = N_{max}$. The state densities for this example are presented in Fig. 4.11. Here, we observe trends similar to those shown in Fig. 4.10 where there is no saturation in state density at low energy.

We take three cases depicted in Fig. 4.11 to illustrate the distribution of many-parton states over the sectors of the Fock-space. The distributions for the $N_{max} = K = 8, 10$ and 12

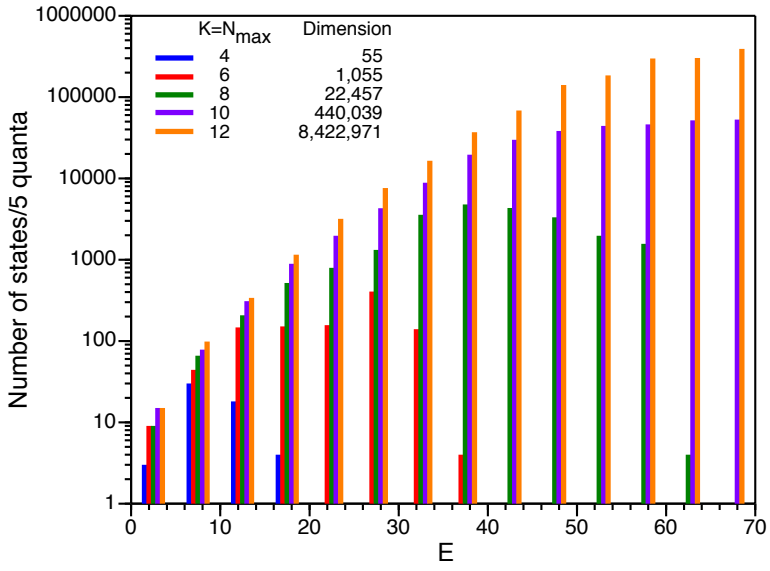

Figure 4.11 State density as a function of dimensionless state energy E from BLFQ for non-interacting QED in a trap with no net charge and for $K = N_{max}$. The dimensions of the resulting matrices are presented in the legend. The states are binned in groups of 5 units of energy (quanta) where each parton carries energy equal to its 2-D oscillator quanta $(2n_i+|m_i|+1)$ divided by its light-front momentum fraction $(x_i = k_i/K)$.

examples are shown in Table 4.1. With increasing cutoff, there is a rapid growth in the number of basis states within each Fock space sector. Overall, there is approximately a factor of 20 increase in the total many-parton basis states with each increase of 2 units in the coordinated cutoff.

Specific cases in Table 4.1 where no basis states may appear in a given Fock space sector may seem puzzling at first. However, they are understandable once the symmetries and constraints are examined. For example, with $N_{max} = K = 8$ there are no states with 4 $f\bar{f}$ pairs since the Pauli principle excludes more than 2 pairs from occupying the lowest N_{max} and K modes. Since two $f\bar{f}$ pairs must be in higher modes, either the total $K = 8$ or $N_{max} = 8$ constraint will be violated by having a total of 4 $f\bar{f}$ pairs.

All our level density results are shown as a function of the dimensionless energy. For the

$f\bar{f}$ pairs / bosons	0	1	2	3	4	5	6	7	8	9	10	Total
0	0	0	210	0	1122	0	67	0	1	0	0	1400
	0	0	495	0	11318	0	2936	0	69	0	1	14819
	0	0	1001	0	73600	0	63315	0	4027	0	69	142013
1	420	1932	8190	1040	588	8	2	0	0	0	0	12180
	990	10512	86856	33632	36672	1604	640	8	2	0	0	170916
	2002	40810	574860	503040	929064	99962	60518	1770	644	8	2	2212680
2	5961	1560	1133	4	1	0	0	0	0	0	0	8659
	64240	59240	97584	4040	1513	4	1	0	0	0	0	226622
	427730	942240	2806624	381608	249825	4928	1565	4	1	0	0	4814525
3	218	0	0	0	0	0	0	0	0	0	0	218
	25584	1528	554	0	0	0	0	0	0	0	0	27666
	808034	222336	200676	2592	602	0	0	0	0	0	0	1234240
4	0	0	0	0	0	0	0	0	0	0	0	0
	16	0	0	0	0	0	0	0	0	0	0	16
	19325	168	20	0	0	0	0	0	0	0	0	19513

Table 4.1 Number of many-parton basis states in each Fock-space sector for three of the $N_{max} = K$ cases depicted in Fig. 4.11. The counts are organized according to the number of fermion-antifermion ($f\bar{f}$) pairs and the number of bosons in each sector. The first line in each $f\bar{f}$ row corresponds to the $N_{max} = K = 8$ case which has a total of 22,457 states, while the second line corresponds to the $N_{max} = K = 10$ case which has a total of 440,039 states. The third line in each $f\bar{f}$ row corresponds to the $N_{max} = K = 12$ case which has a total of 8,422,971 states. In this last case, there is a single 12-boson state not listed to save space. The last column provides the total for that row.

non-interacting theory in BLFQ only the kinetic term of the Hamiltonian contributes and the scale is available through an overall factor $\Lambda^2 = 2M_0\Omega$ as described above. Without interactions and the associated renormalization program, one cannot relate the scales at one set of (K, N_{max}) values to another. Ultimately, one expects saturation will arise with interaction/renormalization physics included as one increases the set of (K, N_{max}) values.

These state densities could serve as input to model the statistical mechanics of the system treated in the microcanonical ensemble. Of course, interactions must be added to make the model realistic at low temperatures where correlations are important. After turning on the interactions, the challenge will be to evaluate observables and demonstrate convergence with respect to the cutoffs (N_{max} and K). Independence of the basis scale, Ω, must also be obtained. These are the standard challenges of taking the continuum limit. We will address these topics in a separate investigation. For the current effort, we present a smooth representation for selected histograms, an exponential fit adopted from the well-known Bethe formula,

$$\rho(E) = b \exp(\sqrt{aE}), \tag{4.17}$$

where the precise values of the fitted constants are provided in the legends. We provide these exponential fits in Figs. 4.8 and 4.9 where the low-lying state density exhibits saturation.

4.3.2 Specific heat

In this section, we will use the state density given in Eqn.(4.17) to find the specific heat of the system.

In the Microcanonical Ensemble, we can obtain the entropy of system from the density of states. The relationship between entropy S and the density of states ρ is given by well-known result:

$$S(E,V) = k\log(\rho(E)). \tag{4.18}$$

Once we obtain entropy, other statistical properties of the whole system can be easily derived. For example, we can calculate the specific heat of the system from the entropy.

To obtain the specific heat, we need to take the derivative of energy with respect to temperature. At first, from Eqn.(4.17) and Eqn.(4.18), we have

$$\frac{1}{T} = \frac{\partial S}{\partial E} = \frac{k\sqrt{a}}{2}E^{-\frac{1}{2}}. \tag{4.19}$$

Then we obtain the relation between energy and temperature which is given by

$$E = \frac{a}{4}k^2T^2. \tag{4.20}$$

Finally we obtain specific heat which is given below

$$c_v = \frac{\partial E}{\partial T} = \frac{a}{2}k^2T. \tag{4.21}$$

From Eqn.(4.21), we obtain the specific heat which shows a linear relationship with temperature. We found it is very close to an ideal Fermi gas. Recall that internal energy of ideal Fermi gas in the Grand Canonical Ensemble is

$$E = -\frac{\partial\log(Z_g)}{\partial\beta} = \sum_p \frac{\epsilon(p)}{e^{\beta(\epsilon(p)-\mu)}+1}. \tag{4.22}$$

If we want to estimate the change in internal energy at a small but finite temperature, one can argue that there will only be changes of electrons close to the Fermi level. Their excitation energy is around kT whereas the relative number of excited states is only $\rho_0(E_F)kT$. Due to $\rho_0(E_F) = \frac{1}{E_F}$, we therefore estimate

$$E = \frac{3}{5} < N > E_F + < N > \rho_0(E_F)(kT)^2 + ... \tag{4.23}$$

At low temperature. This leads then to a specific heat at constant volume

$$c_v = \frac{1}{< N >} \frac{\partial E}{\partial T} = 2k^2 \rho_0(E_F) T = \gamma T, \tag{4.24}$$

where

$$\gamma = \frac{\pi^2}{3} k^2 \rho_0(E_F). \tag{4.25}$$

Now we can compare Eqn.(4.21) and Eqn.(4.24). In Eqn.(4.21), T is dimensionless which corresponds to $\rho_0(E_F)T = \frac{T}{E}$ in Eqn.(4.24). Also we found in Eqn.(4.21) the constant is $\frac{3}{2}$ which is around half of constant in Eqn.(4.24) which is $\frac{\pi^2}{3}$.

4.3.3 Distribution functions

In order to illustrate the potential value of the BLFQ approach, we present light-front momentum distribution functions for two simple toy models, based on results presented in Fig. 4.11. In the first example, we consider a model for a weak coupling regime and, in the second example, we consider a model for strong coupling behavior. In both cases we introduce a simple state that is an equally-weighted superposition of basis states. In the weak coupling case, we retain all basis states below a cutoff ($E_{cut} = 25$) in the dimensionless energy scale of Fig. 4.11 for a given value of $K = N_{max}$. That is, we imagine a situation where only the low-lying unperturbed many-parton basis states mix equally to describe a low-lying physical state of a weakly-coupled physical system. In the strong coupling case we retain all basis states of Fig. 4.11 with equal weights for a given value of $K = N_{max}$. Here, we imagine the coupling is so strong as to overwhelm the unperturbed spectrum and to produce a simple low-lying physical state with equal admixtures of all available basis states. These states, labeled $|\Psi_w\rangle$ and $|\Psi_s\rangle$, where the w ("s") represents "weak" ("strong") respectively, are written as normalized sums over their respective sets of many-parton basis states $|\Phi_j\rangle$ as

$$|\Psi_a\rangle = \frac{1}{\sqrt{D_a}} \sum_j |\Phi_j\rangle. \tag{4.26}$$

where "a" represents "w" or "s" and the sum runs over the D_a respective many-parton states. For our present application to probability distribution functions, the phases of the individual terms in expansion are not relevant so we choose all of them to be positive for simplicity.

Selected light-front momentum distributions $n(x)$ for these two model states are shown in Figs. 4.12 and 4.13. The fermion and antifermion distributions are the same in these limiting examples. Light-front momentum distributions are probability distributions emerging after integration over transverse degrees of freedom. With our present selection of basis states, the light-front momenta take discrete values leading to discrete-valued distributions (histograms). However, for convenience, we present smooth distributions in Figs. 4.12 and 4.13 generated by spline interpolations.

The parton distributions at fixed $N_{max} = K$ satisfy both the normalization condition:

$$\sum_i \int_0^1 n_i(x)dx = \frac{1}{K}\sum_{i,k} n_i(x_k) = 1 \tag{4.27}$$

and total light-front momentum conservation

$$\sum_i \int_0^1 x n_i(x)dx = \frac{1}{K}\sum_{i,k} x_k n_i(x_k) = 1. \tag{4.28}$$

The index i runs over the parton species (fermion, antifermion, boson) and the index k runs over the discrete values of light-front momenta corresponding to the integers in Eqn.(4.4) where $x_k = \frac{k}{K}$.

The top panels of Figs. 4.12 and 4.13 display the light-front momentum distributions at $N_{max} = K = 8$ for the "weak" and "strong" coupling models, respectively. The lower panels present the boson distribution functions for three $N_{max} = K$ values ranging from 8 to 12 for the same models.

The fermion distributions are found to track the boson distributions with increasing $N_{max} = K$ and are not shown in the lower panels. We also comment that the total momentum distribution fractions carried by the separate parton species appear approximately independent of $N_{max} = K$ over the range $8 - 12$. About two-thirds of the total light-front momentum is carried by the fermions plus antifermions. This division is characteristic of both the weak and strong coupling models over the $N_{max} = K = 8 - 12$ range we examined.

The top panel of Fig. 4.13 indicates a peak in the vicinity of the minimum light-front momentum fraction carried by a single parton in this basis, $x = \frac{1}{8}$, for both the fermions and the bosons. This appears to be a characteristic of this strong coupling toy model and is illustrated in the lower panel of the same figure where the peaks in the boson light-front momentum distributions appear to track well with the inverse of $N_{max} = K$. Clearly, with this toy model the distribution functions do not converge with increasing N_{max} and K.

For comparison, we note that with the weak coupling toy model the peaks of the boson distributions shown in Fig.4.12 appear to be stable with increasing N_{max} and K, and the distribution function appears to be reasonably well converged at $N_{max} = K = 12$. Based on these observations we anticipate good convergence for weakly interacting theories like QED.

The lack of convergence of our strong coupling toy model may be worrisome for applications in QCD, but one should keep in mind that this toy model is far from realistic: all basis states are retained with equal weight. Nevertheless, it is interesting to consider the trends of this model with increasing $N_{max} = K$. For background, one may recall that deep-inelastic lepton scattering from a hadron in the scaling region $Q^2 \to \infty$ provides a measure of the hadron's charged quark distribution functions. With more detailed resolution provided by the virtual photon exchange (increasing Q leads to shorter wavelengths), experiments reveal that the charged quark distributions evolve to lower values of light-front momentum fraction, x. The pattern shown in the lower panel of Fig. 4.13 with increasing $N_{max} = K$ is reminiscent of this experimental trend with increasing Q. Given the simplicity of the strong interaction model, one may infer that the evolution of multi-parton phase space with increasing $N_{max} = K$ could play a significant role in the evolution of light-front momentum distribution functions with improved resolution through increasing Q.

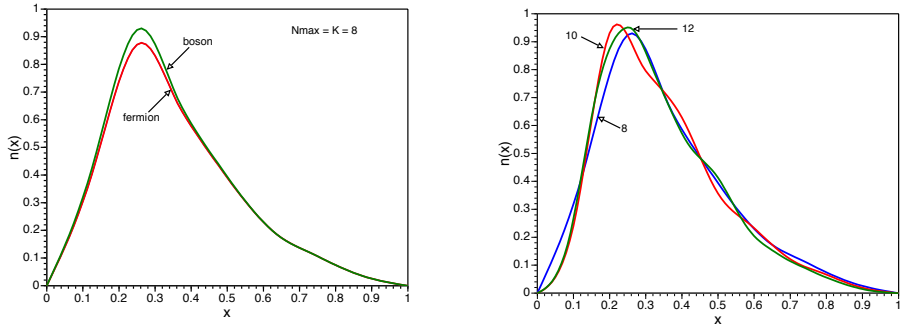

Figure 4.12 Light front momentum distribution functions for states representing a weak coupling paradigm. The top panel displays the distributions at $N_{max} = K = 8$. The antifermion distribution is the same as the fermion distribution. The total momentum fraction carried by the fermion plus antifermion distribution is 0.66 while the boson distribution carries the remaining fraction 0.34. The bottom panel displays the boson distributions at three different values of $N_{max} = K$ that are labeled.

4.3.4 Extension to color without color restriction

We can extend the approach to QCD by implementing the SU(3) color degree of freedom for each parton - 3 colors for each fermion and 8 for each boson as we have discussed in previous chapters. For simplicity, we restrict the present discussion to the situation where identical fermions occupy distinct space-spin single-particle modes. The case where we allow multiple space-spin occupancies by identical fermions leads to color space restrictions. We will address this additional complexity in the following subsection.

We considered two versions of implementing the global color-singlet constraint for the restricted situation under discussion here. In both cases we enumerate the color space states to integrate with each space-spin state of the corresponding partonic character.

In the first case, we follow Ref. [33] by enumerating parton states with all possible values of SU(3) color. Thus each space-spin fermion state goes over to three space-spin-color states. Similarly, each space-spin boson state generates a multiplicity of eight states when SU(3) color is included. We then construct all many-parton states having zero color projection. Within this basis one will have both global color singlet and color non-singlet states. The global color-

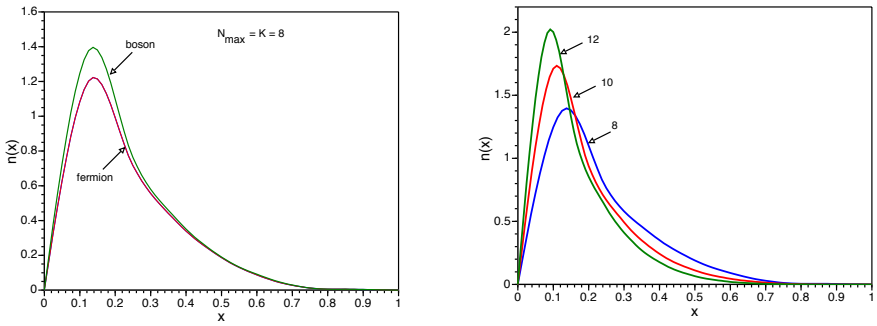

Figure 4.13 Light front momentum distribution functions for states representing a strong coupling paradigm. The top panel displays the distributions at $N_{max} = K = 8$. The antifermion distribution is the same as the fermion distribution. The total momentum fraction carried by the fermion plus antifermion distribution is 0.65 while the boson distribution carries the remaining fraction 0.35. The bottom panel displays the boson distributions at three different values of $N_{max} = K$ that are labeled.

singlet states are then isolated by adding a Lagrange multiplier term in many-parton color space to the Hamiltonian so that the unphysical color non-singlet states are pushed higher in the spectrum away from the physical color single states. To evaluate the increase in basis space dimension arising from this treatment of color, we enumerate the resulting color-singlet projected color space states and display the results as the upper curves in Fig. 3.1.

In the second case, we restrict the basis space to global color singlets and this results in the lower curves in Fig. 3.1. The second method produces a typical factor of 30-40 lower multiplicity at the upper ends of these curves at the cost of increased computation time for matrix elements of the interacting Hamiltonian. That is, each interacting matrix element in the global color-singlet basis is a transformation of a submatrix in the zero color projection basis. Either implementation dramatically increases the state density over the case of QED, but the use of a global color-singlet constraint is clearly more effective in minimizing the explosion in basis space states.

We note that, for the pure multi-fermion basis space sector, shown in the upper left panel of Fig. 3.1, we could have produced the lower curve using methods introduced and applied

successfully in 1 + 1 dimensional QCD [34]. That is, the number of global color singlets for a given fermion-only basis state, with other (non-color) quantum numbers specified, is independent of the number of spatial dimensions provided there is at least one.

As the first example to implement the global color-singlet constraint, we consider the system with no net charge and $K = N_{max} = 4$. The state density for this system without considering color space was presented in Fig.4.11. We now implement the global color-singlet constraint and present the new state density in Fig.4.14 where we compare the previous state densities obtained without considering the color degree of freedom.

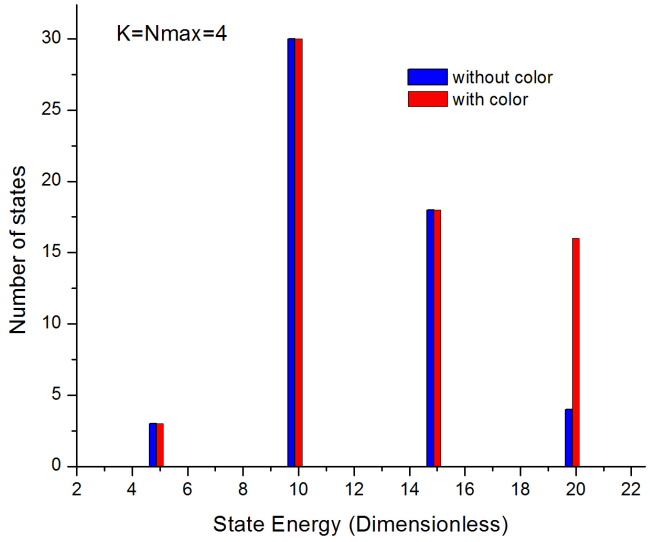

Figure 4.14 State density as a function of dimensionless state energy E from BLFQ for non-interacting QCD in a trap with no net charge and for a selection of $K = N_{max} = 4$.

When we compare Fig.4.14 with Fig.4.11, we found that there are a total of 67 states instead of 55 states after we implement the global color-singlet constraint. With global color-singlet constraint, one state with 4 gluons needs to be multiplied by 8 because in color space, 4 gluons can form 8 color singlet states. Two states with one quark, one antiquark and two gluons need to be multiplied by 3 because in color space it can form 3 color singlet states. Finally, one state with two quarks and two antiquarks needs to be multiplied by 2 . Therefore, there are 12 more states than the 55 states without the addition of the color degree of freedom. Furthermore, we found that the 12 additional states are all sitting in the highest energy bin.

Significant new features arise when we consider the global color-singlet constraint for the same system with $K = N_{max} = 6$. The comparison of state densities without and with the color degree of freedom is presented in Fig.4.15. After we consider the global color-singlet constraint, there are 1777 states instead of original 1055 states without the addition of the color degree of freedom.

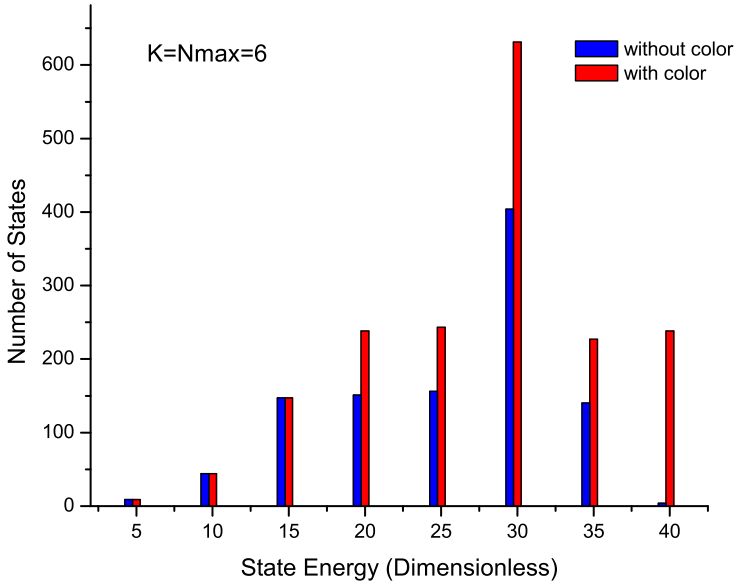

Figure 4.15 State density as a function of dimensionless state energy E from BLFQ for non-interacting QCD in a trap with no net charge and for a selection of $K = N_{max} = 6$. The blue histograms are the distribution of state density without global color-singlet constraint. The red histograms are the distribution of state density with global color-singlet constraint.

4.3.5 Extension to color with color restriction

In the last section, we have seen how the global color-singlet constraint modifies the state density: there are more states generated. However we have not yet considered the case where we allow multiple space-spin occupancies by identical fermions. This case leads to color space restrictions. For example, if two identical fermions are in same space-spin configuration, they must have different color in color space in order to respect the Pauli principle.

To see how state density changes when we add the allowed states with space-spin degeneracy and include the appropriate color singlet states, we again consider the system with no net charge and for a selection of $K = N_{max} = 6$. When we allow multiple space-spin occupancies by identical fermions, there are 60 more states generated prior to including the color degree of freedom. For example, we now include the states where two fermions are in the same space-spin

configuration and two anti-fermions are in the same space-spin configuration. Once we include the color singlet configurations for these added states, the state density increases further and the results are presented in Fig.4.16.

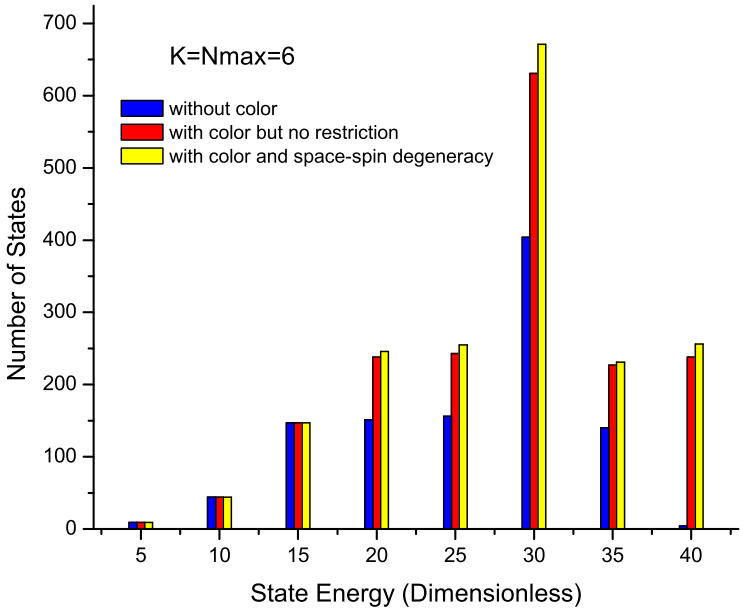

Figure 4.16 State density as a function of dimensionless state energy E from BLFQ for non-interacting QCD in a trap with no net charge and for a selection of $K = N_{max} = 6$. The blue histograms are the distribution of state density without global color-singlet constraint. The red histograms are the distribution of state density with global color-singlet constraint but no allowance to have multiple space-spin occupancies by identical fermions. The yellow histograms are the distribution of state density with global color-singlet constraint also with allowance to have multiple space-spin occupancies by identical fermions.

CHAPTER 5. SUMMARY AND OUTLOOK

Quantum Chromodynamics (QCD) is a fundamental theory of the strong interaction. At short distance, due to asymptotic freedom, the perturbative calculation is successful. However, when the coupling constant becomes larger, the perturbative calculation fails and a suitable non-perturbative method must be found. Hamiltonian light-front quantum field theory constitutes a framework for the non-perturbative solution of invariant masses and correlated parton amplitudes of self-bound systems.

By choosing the light-front gauge and adopting a basis function representation, we obtain a large, sparse, Hamiltonian matrix for mass eigenstates of gauge theories. Full covariance is recovered in the continuum limit, the infinite matrix limit. There is considerable freedom in the choice of the orthonormal and complete set of basis functions with convenience and convergence rates providing key considerations. In this thesis we use a two-dimensional harmonic oscillator basis for transverse modes that corresponds with eigensolutions of the soft-wall AdS/QCD model obtained from light-front holography. We outline our approach, present illustrative features of some non-interacting systems in a cavity and discuss the computational challenges.

Following successful methods of ab initio nuclear many-body theory, we have introduced a basis light-front quantization (BLFQ) approach to Hamiltonian quantum field theory and illustrated some of its key features with a cavity mode treatment of massless non-interacting QED. Cavity mode QED, with a 2D harmonic oscillator for the transverse modes and longitudinal modes chosen with periodic boundary conditions, exhibits the expected dramatic rise in many-parton basis states as the cutoffs are elevated. With the non-intracting cavity-mode Hamiltonian, we obtain the state density distributions at various choices of the regulators. These basis state densities provide initial elements of a quantum statistical mechanics ap-

proach to systems treated in the BLFQ approach. We then illustrated the access to light front momentum distribution functions in this approach with simple models of wave functions that reflect possible interaction effects. In order to extend our method to QCD, we have evaluated two methods for treating the color degree of freedom. Since large sparse matrices will emerge, we argue that it is more efficient in storage requirements to adopt multi-parton basis states that are global color singlets and we presented sample measures of the efficiency gains over basis states with color-singlet projection alone. To achieve this savings in storage (reduced matrix size) we will incur an increase in the computational effort for the non-vanishing matrix elements.

APPENDIX A. COLOR ALGEBRA

Gell-Mann matrices acting on quark color states

We have employed the feature that the operator F^2 gives zero when acting on the color singlet states, and positive for all color-nonsinglet states. In this appendix, we will see what we can obtain with the eight Gell-Mann matrices acting on quark color states separately. In the calculations, we used these to construct the color singlet state.

We begin with these definitions.

$$\begin{aligned} I_+ &= F_1 + iF_2, I_- = F_1 - iF_2, \\ T_3 &= F_3, \\ U_+ &= F_6 + iF_7, U_- = F_6 - iF_7, \\ V_+ &= F_4 + iF_5, V_- = F_4 - iF_5, \\ Y &= \frac{2}{\sqrt{3}} F_8. \end{aligned} \tag{A.1}$$

Now let us define the quark color state by using two quantum number T_3 and Y. Therefore using $SU(3)$ algebra, we have

$$\begin{aligned} F_3|t_3, y\rangle &= T_3|t_3, y\rangle, \\ F_8|t_3, y\rangle &= \frac{\sqrt{3}}{2} y|t_3, y\rangle, \\ I_+|t_3, y\rangle &= \sqrt{(t - t_3)(t + t_3 + 1)}|t_3 + 1, y\rangle, \\ I_-|t_3, y\rangle &= \sqrt{(t + t_3)(t - t_3 + 1)}|t_3 - 1, y\rangle. \end{aligned} \tag{A.2}$$

Using the relation between F_1, F_2 and I_+, I_- and also the result $t = \frac{1}{2}$, we obtain

$$F_1|t_3, y\rangle = \frac{1}{2}(\sqrt{(\frac{1}{2} - t_3)(\frac{1}{2} + t_3 + 1)}|t_3 + 1, y\rangle$$

$$
\begin{aligned}
& +\sqrt{(\frac{1}{2}-t_3)(\frac{1}{2}+t_3+1)}|t_3+1,y\rangle)\delta_{|t_3|,\frac{1}{2}}, \\
F_2|t_3,y\rangle &= \frac{1}{2i}(\sqrt{(\frac{1}{2}-t_3)(\frac{1}{2}+t_3+1)}|t_3+1,y\rangle \\
& -\sqrt{(\frac{1}{2}-t_3)(\frac{1}{2}+t_3+1)}|t_3+1,y\rangle)\delta_{|t_3|,\frac{1}{2}}. \qquad \text{(A.3)}
\end{aligned}
$$

Then we can define two more new quantum numbers

$$
V_3 = \frac{3}{4}y + \frac{1}{2}t_3,\ U_3 = \frac{3}{4}y - \frac{1}{2}t_3. \qquad \text{(A.4)}
$$

Therefore three quarks carry these two quantum numbers seperately. We have

$$
\begin{aligned}
V_3^R &= \frac{1}{2}, V_3^G = 0, V_3^B = -\frac{1}{2}, \\
U_3^R &= 0, U_3^G = \frac{1}{2}, U_3^B = -\frac{1}{2}. \qquad \text{(A.5)}
\end{aligned}
$$

Finally if we do a similar calculation as for I_+ and I_-, we can obtain the result

$$
\begin{aligned}
F_4|t_3,y\rangle &= \frac{1}{2}(\sqrt{(\frac{1}{2}-\frac{1}{2}t_3-\frac{3}{4}y)(\frac{1}{2}+\frac{1}{2}t_3+\frac{3}{4}y+1)}|t_3+\frac{1}{2},y+1\rangle \\
& +\sqrt{(\frac{1}{2}+\frac{1}{2}t_3+\frac{3}{4}y)(\frac{1}{2}-\frac{1}{2}t_3-\frac{3}{4}y+1)}|t_3-\frac{1}{2},y-1\rangle)\delta_{|\frac{1}{2}t_3+\frac{3}{4}y|,\frac{1}{2}}, \\
F_5|t_3,y\rangle &= \frac{1}{2i}(\sqrt{(\frac{1}{2}-\frac{1}{2}t_3-\frac{3}{4}y)(\frac{1}{2}+\frac{1}{2}t_3+\frac{3}{4}y+1)}|t_3+\frac{1}{2},y+1\rangle \\
& -\sqrt{(\frac{1}{2}+\frac{1}{2}t_3+\frac{3}{4}y)(\frac{1}{2}-\frac{1}{2}t_3-\frac{3}{4}y+1)}|t_3-\frac{1}{2},y-1\rangle)\delta_{|\frac{1}{2}t_3+\frac{3}{4}y|,\frac{1}{2}}, \\
F_6|t_3,y\rangle &= \frac{1}{2}(\sqrt{(\frac{1}{2}+\frac{1}{2}t_3-\frac{3}{4}y)(\frac{1}{2}-\frac{1}{2}t_3+\frac{3}{4}y+1)}|t_3-\frac{1}{2},y+1\rangle \\
& +\sqrt{(\frac{1}{2}-\frac{1}{2}t_3+\frac{3}{4}y)(\frac{1}{2}+\frac{1}{2}t_3-\frac{3}{4}y+1)}|t_3+\frac{1}{2},y-1\rangle)\delta_{|-\frac{1}{2}t_3+\frac{3}{4}y|,\frac{1}{2}}, \\
F_7|t_3,y\rangle &= \frac{1}{2i}(\sqrt{(\frac{1}{2}+\frac{1}{2}t_3-\frac{3}{4}y)(\frac{1}{2}-\frac{1}{2}t_3+\frac{3}{4}y+1)}|t_3-\frac{1}{2},y+1\rangle \\
& -\sqrt{(\frac{1}{2}-\frac{1}{2}t_3+\frac{3}{4}y)(\frac{1}{2}+\frac{1}{2}t_3-\frac{3}{4}y+1)}|t_3+\frac{1}{2},y-1\rangle)\delta_{|-\frac{1}{2}t_3+\frac{3}{4}y|,\frac{1}{2}}. \qquad \text{(A.6)}
\end{aligned}
$$

Color matrices acting on gluon color states

In this section, we show what we can obtain when the eight color matrices act on gluon color states.

Since, in the adjoint representation, gluon eigenstates g_3 and g_8 cannot be completely distinguished by two quantum numbers t_3 and y (both of them have the same quantum $t_3 = 0$

and $y = 0$), we have to add one more quantum number t when we express the color eigenstates. Therefore we can see that g_3 has quantum number $t = 1$ and g_8 has quantum number $t = 0$.

In the previous section, we have used the following operators:I_+, I_-, V_+, V_-, U_+ and U_-. In this section, we still take advantage of these operators. And we notice that for I_+ and I_-, we have

$$\begin{aligned}
I_+ g_2 &\rightarrow g_3, I_+ g_3 \rightarrow g_1, I_+ g_1 = 0, \\
I_- g_1 &\rightarrow g_3, I_- g_3 \rightarrow g_2, I_- g_2 = 0, \\
I_+ g_6 &\rightarrow g_4, I_+ g_4 = 0, \\
I_- g_4 &\rightarrow g_6, I_- g_6 = 0, \\
I_+ g_5 &\rightarrow g_7, I_+ g_7 = 0, \\
I_- g_7 &\rightarrow g_5, I_- g_5 = 0.
\end{aligned} \tag{A.7}$$

For V_+ and V_-, we have

$$\begin{aligned}
V_+ g_7 &\rightarrow g_1, V_+ g_1 = 0, \\
V_- g_1 &\rightarrow g_7, V_- g_7 = 0, \\
V_+ g_2 &\rightarrow g_6, V_+ g_6 = 0, \\
V_- g_6 &\rightarrow g_2, V_- g_2 = 0, \\
V_+ g_5 &\rightarrow g_3 + g_8, V_+(g_3 + g_8) \rightarrow g_4, V_+ g_4 = 0, \\
V_- g_4 &\rightarrow g_3 + g_8, V_-(g_3 + g_8) \rightarrow g_5, V_- g_5 = 0.
\end{aligned} \tag{A.8}$$

For U_+ and U_-, we have

$$\begin{aligned}
U_+ g_1 &\rightarrow g_4, U_+ g_4 = 0, \\
U_- g_4 &\rightarrow g_1, U_- g_1 = 0, \\
U_+ g_5 &\rightarrow g_2, U_+ g_2 = 0, \\
U_- g_2 &\rightarrow g_5, U_- g_5 = 0, \\
U_+ g_7 &\rightarrow g_3 + g_8, U_+(g_3 + g_8) \rightarrow g_6, U_+ g_6 = 0, \\
U_- g_6 &\rightarrow g_3 + g_8, U_-(g_3 + g_8) \rightarrow g_7, U_- g_7 = 0.
\end{aligned} \tag{A.9}$$

Using procedures we used when we calculated the quark color states, we can obtain the results which are given below

$$
\begin{aligned}
F_1|t_3,t,y\rangle &= \frac{y}{2}\delta_{|t_3|,\frac{1}{2}}(\sqrt{(\frac{1}{2}-t_3)(\frac{1}{2}+t_3+1)}|t_3+1,t,y\rangle+\sqrt{(\frac{1}{2}+t_3)(\frac{1}{2}-t_3+1)}|t_3-1,t,y\rangle)\\
&+\frac{1}{2}\delta_{t,1}\delta_{y,0}((-1)^{1-t_3}(1-t_3)|t_3+1,t,y\rangle+(-1)^{t_3}(1+t_3)|t_3-1,t,y\rangle)\\
&+\frac{1}{2}\delta_{t,0}\delta_{y,0}(t_3+y)|t_3,t,y\rangle,\\
F_2|t_3,t,y\rangle &= \frac{y}{2i}\delta_{|t_3|,\frac{1}{2}}(\sqrt{(\frac{1}{2}-t_3)(\frac{1}{2}+t_3+1)}|t_3+1,t,y\rangle-\sqrt{(\frac{1}{2}+t_3)(\frac{1}{2}-t_3+1)}|t_3-1,t,y\rangle)\\
&+\frac{1}{2i}\delta_{t,1}\delta_{y,0}((-1)^{1-t_3}(1-t_3)|t_3+1,t,y\rangle-(-1)^{t_3}(1+t_3)|t_3-1,t,y\rangle)\\
&+\frac{1}{2i}\delta_{t,0}\delta_{y,0}(t_3-y)|t_3,t,y\rangle,\\
F_3|t_3,t,y\rangle &= t_3|t_3,t,y\rangle,\\
F_4|t_3,t,y\rangle &= \delta_{|\frac{3}{4}y+\frac{1}{2}t_3|,\frac{1}{2}}(\frac{1}{2}t_3-\frac{1}{4}y)(\sqrt{(\frac{1}{2}-\frac{3}{4}y-\frac{1}{2}t_3)(\frac{1}{2}+\frac{3}{4}y+\frac{1}{2}t_3+1)}|t_3+\frac{1}{2},t,y+1\rangle\\
&+\sqrt{(\frac{1}{2}+\frac{3}{4}y+\frac{1}{2}t_3)(\frac{1}{2}-\frac{3}{4}y-\frac{1}{2}t_3+1)}|t_3-\frac{1}{2},t,y-1\rangle)\\
&+\delta_{t_3,0}\delta_{y,0}\delta_{t,1}((-\frac{1}{4})|t_3+\frac{1}{2},t-\frac{1}{2},y+1\rangle+\frac{1}{4}|t_3-\frac{1}{2},t-\frac{1}{2},y-1\rangle)\\
&+\delta_{t_3,\frac{1}{2}}\delta_{y,1}\delta_{t,\frac{1}{2}}((-\frac{1}{2})|-t_3+\frac{1}{2},t+\frac{1}{2},y-1\rangle-\frac{\sqrt{3}}{2}|-t_3+\frac{1}{2},t-\frac{1}{2},y-1\rangle)\\
&+\delta_{t_3,-\frac{1}{2}}\delta_{y,-1}\delta_{t,\frac{1}{2}}(\frac{1}{2}|-t_3+\frac{1}{2},t+\frac{1}{2},y-1\rangle+\frac{\sqrt{3}}{2}|-t_3+\frac{1}{2},t-\frac{1}{2},y-1\rangle)\\
&+\delta_{t_3,0}\delta_{y,0}\delta_{t,0}((-\frac{\sqrt{3}}{4})|t_3+\frac{1}{2},t+\frac{1}{2},y+1\rangle+\frac{\sqrt{3}}{4}|t_3-\frac{1}{2},t+\frac{1}{2},y-1\rangle),\\
F_5|t_3,t,y\rangle &= \delta_{|\frac{3}{4}y+\frac{1}{2}t_3|,\frac{1}{2}}(\frac{1}{2i}t_3-\frac{1}{4i}y)(\sqrt{(\frac{1}{2}-\frac{3}{4}y-\frac{1}{2}t_3)(\frac{1}{2}+\frac{3}{4}y+\frac{1}{2}t_3+1)}|t_3+\frac{1}{2},t,y+1\rangle\\
&-\sqrt{(\frac{1}{2}+\frac{3}{4}y+\frac{1}{2}t_3)(\frac{1}{2}-\frac{3}{4}y-\frac{1}{2}t_3+1)}|t_3-\frac{1}{2},t,y-1\rangle)\\
&+\delta_{t_3,0}\delta_{y,0}\delta_{t,1}(\frac{i}{4}|t_3+\frac{1}{2},t-\frac{1}{2},y+1\rangle+\frac{i}{4}|t_3-\frac{1}{2},t-\frac{1}{2},y-1\rangle)\\
&+\delta_{t_3,\frac{1}{2}}\delta_{y,1}\delta_{t,\frac{1}{2}}((-\frac{i}{2})|-t_3+\frac{1}{2},t+\frac{1}{2},y-1\rangle-\frac{\sqrt{3}i}{2}|-t_3+\frac{1}{2},t-\frac{1}{2},y-1\rangle)\\
&+\delta_{t_3,-\frac{1}{2}}\delta_{y,1}\delta_{t,\frac{1}{2}}(-\frac{i}{2}|-t_3+\frac{1}{2},t+\frac{1}{2},y-1\rangle-\frac{\sqrt{3}i}{2}|-t_3+\frac{1}{2},t-\frac{1}{2},y-1\rangle)\\
&+\delta_{t_3,0}\delta_{y,0}\delta_{t,0}((\frac{\sqrt{3}i}{4})|t_3+\frac{1}{2},t+\frac{1}{2},y+1\rangle+\frac{\sqrt{3}i}{4}|t_3-\frac{1}{2},t+\frac{1}{2},y-1\rangle),\\
F_6|t_3,t,y\rangle &= \delta_{|\frac{3}{4}y-\frac{1}{2}t_3|,\frac{1}{2}}(-\frac{1}{2}t_3-\frac{1}{4}y)(\sqrt{(\frac{1}{2}-\frac{3}{4}y+\frac{1}{2}t_3)(\frac{1}{2}+\frac{3}{4}y-\frac{1}{2}t_3+1)}|t_3-\frac{1}{2},t,y+1\rangle\\
&+\sqrt{(\frac{1}{2}+\frac{3}{4}y-\frac{1}{2}t_3)(\frac{1}{2}-\frac{3}{4}y+\frac{1}{2}t_3+1)}|t_3+\frac{1}{2},t,y-1\rangle)\\
&+\delta_{t_3,0}\delta_{y,0}\delta_{t,1}(\frac{1}{4}|t_3-\frac{1}{2},t-\frac{1}{2},y+1\rangle-\frac{1}{4}|t_3+\frac{1}{2},t-\frac{1}{2},y-1\rangle)
\end{aligned}
$$

$$
\begin{aligned}
&+\delta_{t_3,-\frac{1}{2}}\delta_{y,1}\delta_{t,\frac{1}{2}}(\frac{1}{2}|t_3+\frac{1}{2},t+\frac{1}{2},y-1\rangle-\frac{\sqrt{3}}{2}|t_3+\frac{1}{2},t-\frac{1}{2},y-1\rangle)\\
&+\delta_{t_3,\frac{1}{2}}\delta_{y,-1}\delta_{t,\frac{1}{2}}((-\frac{1}{2})|t_3+\frac{1}{2},t+\frac{1}{2},y-1\rangle+\frac{\sqrt{3}}{2}|t_3+\frac{1}{2},t-\frac{1}{2},y-1\rangle)\\
&+\delta_{t_3,0}\delta_{y,0}\delta_{t,0}((-\frac{\sqrt{3}}{4})|t_3-\frac{1}{2},t+\frac{1}{2},y+1\rangle+\frac{\sqrt{3}}{4}|t_3+\frac{1}{2},t+\frac{1}{2},y-1\rangle),\\
F_7|t_3,t,y\rangle &= \delta_{|\frac{3}{4}y-\frac{1}{2}t_3|,\frac{1}{2}}(-\frac{1}{2i}t_3-\frac{1}{4i}y)(\sqrt{(\frac{1}{2}-\frac{3}{4}y+\frac{1}{2}t_3)(\frac{1}{2}+\frac{3}{4}y-\frac{1}{2}t_3+1)}|t_3-\frac{1}{2},t,y+1\rangle\\
&-\sqrt{(\frac{1}{2}+\frac{3}{4}y-\frac{1}{2}t_3)(\frac{1}{2}-\frac{3}{4}y+\frac{1}{2}t_3+1)}|t_3+\frac{1}{2},t,y-1\rangle)\\
&+\delta_{t_3,0}\delta_{y,0}\delta_{t,1}((-\frac{i}{4}|t_3-\frac{1}{2},t-\frac{1}{2},y+1\rangle-\frac{i}{4}|t_3+\frac{1}{2},t-\frac{1}{2},y-1\rangle)\\
&+\delta_{t_3,-\frac{1}{2}}\delta_{y,1}\delta_{t,\frac{1}{2}}(\frac{i}{2}|t_3+\frac{1}{2},t+\frac{1}{2},y-1\rangle-\frac{\sqrt{3}i}{2}|t_3+\frac{1}{2},t-\frac{1}{2},y-1\rangle)\\
&+\delta_{t_3,\frac{1}{2}}\delta_{y,-1}\delta_{t,\frac{1}{2}}((-\frac{i}{2})|t_3+\frac{1}{2},t+\frac{1}{2},y-1\rangle-\frac{\sqrt{3}i}{2}|t_3+\frac{1}{2},t-\frac{1}{2},y-1\rangle)\\
&+\delta_{t_3,0}\delta_{y,0}\delta_{t,0}((\frac{\sqrt{3}i}{4})|t_3-\frac{1}{2},t+\frac{1}{2},y+1\rangle+\frac{\sqrt{3}i}{4}|t_3+\frac{1}{2},t+\frac{1}{2},y-1\rangle),\\
F_8|t_3,t,y\rangle &= \frac{\sqrt{3}}{2}y|t_3,t,y\rangle. \qquad \text{(A.10)}
\end{aligned}
$$

APPENDIX B. TWO-DIMENSIONAL HARMONIC OSCILLATOR

Consider the 2-dimensional harmonic oscillator described by the following equation:

$$(\frac{p_x^2+p_y^2}{2\,M}+\frac{1}{2}M\Omega^2\,(x^2+y^2))\Psi \;\;=\;\; E\,\Psi. \tag{B.1}$$

Explicitly, with units $\hbar = c = 1$, we can rewrite the above equation as the equation in Cartesian coordinates:

$$\Big[-\frac{1}{2\,M}\left(\frac{\partial^2}{\partial x^2}+\frac{\partial^2}{\partial y^2}\right)+\frac{1}{2}k(x^2+y^2)\Big]\Psi(x,y) \;\;=\;\; E\,\Psi(x,y), \tag{B.2}$$

or in 2-dimensional polar coordinates:

$$\Big[-\frac{1}{2\,M}\left(\frac{\partial^2}{\partial \rho^2}+\frac{1}{\rho}\frac{\partial}{\partial \rho}+\frac{1}{\rho^2}\frac{\partial^2}{\partial \phi^2}\right)+\frac{1}{2}k\,\rho^2\Big]\Psi(\rho,\phi) \;\;=\;\; E\,\Psi(\rho,\phi), \tag{B.3}$$

where

$$k \;\;=\;\; M\Omega^2, \tag{B.4}$$

$$\rho \;\;=\;\; \sqrt{x^2+y^2}, \tag{B.5}$$

and the polar angle ϕ running from 0 to 2π.

Separation of variables in polar coordinates

Let $\Psi(\rho,\phi) = f(\rho)\chi(\phi)$, then

$$\left[\frac{\rho^2}{f(\rho)}\,\frac{\partial^2 f(\rho)}{\partial \rho^2}+\frac{\rho}{f(\rho)}\,\frac{\partial f(\rho)}{\partial \rho}+2\,M\,\rho^2\,\left(E-\frac{1}{2}\,k\,\rho^2\right)\right]+\frac{1}{\chi(\phi)}\frac{\partial^2\chi(\phi)}{\partial\phi^2} \;\;=\;\; 0, \tag{B.6}$$

provided that neither $f(\rho)$ nor $\chi(\phi)$ vanishes.

The angular wavefunction $\chi(\phi)$ is the solution of

$$\frac{\partial^2\chi(\phi)}{\partial\phi^2} \;\;=\;\; -C\,\chi(\phi). \tag{B.7}$$

Furthermore, we need to put periodic constraint on ϕ: $\chi(\phi + 2\pi) = \chi(\phi)$. Therefore, a solution of the angular differential equation is

$$\chi(\phi) \;=\; \mathcal{A}\,\mathrm{e}^{i\,m\,\phi}, \tag{B.8}$$

with $m^2 = C$ and m has to be integer due to the periodicity of χ. The constant $\mathcal{A}$ is an arbitrary nonzero constant.

Radial wavefunction

With the solution for the angular part of the wavefunction in Eqn.(B8), the equation for the radial part becomes

$$\left[\frac{\rho^2}{f(\rho)}\,\frac{\partial^2 f(\rho)}{\partial\rho^2} + \frac{\rho}{f(\rho)}\,\frac{\partial f(\rho)}{\partial\rho} + 2\,M\,\rho^2\,\left(E - \frac{1}{2}\,k\,\rho^2\right)\right] - m^2 \;=\; 0, \tag{B.9}$$

or equivalently

$$\frac{\partial^2 f(\rho)}{\partial\rho^2} + \frac{1}{\rho}\,\frac{\partial f(\rho)}{\partial\rho} + 2\,M\,\left(E - \frac{1}{2}\,k\,\rho^2\right)\,f(\rho) - \frac{m^2}{\rho^2}\,f(\rho) \;=\; 0. \tag{B.10}$$

Anticipating that there will be discrete energy levels, we can define these levels by

$$E_n \;=\; (2\,n + |m| + 1)\Omega. \tag{B.11}$$

Then the radial differential equation can be written as

$$\frac{\partial^2 f(\rho)}{\partial\rho^2} + \frac{1}{\rho}\frac{\partial f(\rho)}{\partial\rho} + (4\,n + 2\,|m| + 2)M\,\Omega\,f(\rho) - M^2\,\Omega^2\,\rho^2\,f(\rho) - \frac{m^2}{\rho^2}f(\rho) \;=\; 0 \tag{B.12}$$

Dividing both sides by $M\,\Omega$ in the equation above, we obtain

$$\frac{\partial^2 f(\rho)}{M\Omega\partial\rho^2} + \frac{1}{M\Omega\rho}\frac{\partial f(\rho)}{\partial\rho} + (4n + 2|m| + 2)f(\rho) - M\Omega\rho^2 f(\rho) - \frac{m^2}{M\Omega\rho^2}f(\rho) \;=\; 0. \tag{B.13}$$

Defining $t = \sqrt{M\,\Omega}\,\rho$, we obtain

$$\frac{\partial^2 f(t)}{\partial t^2} + \frac{1}{t}\,\frac{\partial f(t)}{\partial t} + (4\,n + 2\,|m| + 2)\,f(t) - t^2\,f(t) - \frac{m^2}{t^2}\,f(t) \;=\; 0. \tag{B.14}$$

Next, if we define

$$f(t) \;=\; t^{-\frac{1}{2}}\,h(t), \tag{B.15}$$

then, we have

$$f''(t) + \frac{1}{t} f'(t) \;=\; \frac{1}{4} t^{-\frac{5}{2}}\; h(t) + t^{-\frac{1}{2}}\; h''(t). \tag{B.16}$$

In this notation, the differential equation Eqn. (B.14) can be rewritten as

$$\frac{\partial^2 h(t)}{\partial t^2} + (4\,n + 2\,|m| + 2)\, h(t) - t^2\, h(t) + \frac{1 - 4\,m^2}{4\,t^2}\, h(t) \;=\; 0. \tag{B.17}$$

The solution of Eq. (B.14) is

$$f(t) \;=\; t^{-\frac{1}{2}}\; h(t) \;=\; \mathcal{N}\, \mathrm{e}^{-t^2/2}\;\; t^{|m|}\;\; L_n^{|m|}(t^2), \tag{B.18}$$

or in terms of $\rho = t/\sqrt{M\,\Omega}$

$$f(\rho) \;=\; \mathcal{N}\, \mathrm{e}^{-M\,\Omega\,\rho^2/2}\;\left(\sqrt{M\,\Omega}\;\rho\right)^{|m|}\;\; L_n^{|m|}(M\,\Omega\,\rho^2). \tag{B.19}$$

Orthonormality

The wavefunctions $\Psi_{n,m}(\rho,\phi) = f_{n,m}(\rho)\chi_m(\phi)$ are normalized according to:

$$\langle nm|n'm'\rangle \;=\; \int_0^\infty \int_0^{2\pi} \rho\, d\rho\; d\phi\; \Psi_{n,m}(\rho,\phi)^*\; \Psi_{n',m'}(\rho,\phi) \;=\; \delta_{n,n'}\; \delta_{m,m'}. \tag{B.20}$$

After the separation into the radial wavefunction

$$f_{n,m}(\rho) \;=\; \mathcal{N}\, \mathrm{e}^{-M\,\Omega\,\rho^2/2}\;\left(\sqrt{M\,\Omega}\;\rho\right)^{|m|}\;\; L_n^{|m|}(M\,\Omega\,\rho^2), \tag{B.21}$$

and the angular wavefunction

$$\chi_m(\phi) \;=\; \frac{1}{\sqrt{2\pi}}\, \mathrm{e}^{i\,m\,\phi}, \tag{B.22}$$

it is straightforward to prove orthogonality as follows. First for the angular wavefunction, we have

$$\int_0^{2\pi} d\phi\; \chi_m(\phi)^*\; \chi_{m'}(\phi) \;=\; \delta_{m,m'}. \tag{B.23}$$

Next we know already that the angular wavefunctions are orthogonal for $m \neq m'$. Therefore we can safely take those quantum numbers equal for the radial wavefunction

$$\int_0^\infty \rho\, d\rho f_{n,m}(\rho)^* f_{n',m}(\rho)$$

$$
\begin{aligned}
&= \int_0^\infty \rho\, d\rho \mathcal{N}\mathcal{N}^* \mathrm{e}^{-M\Omega\rho^2} \left(M\Omega\rho^2\right)^{|m|} L_{n'}^{|m|}(M\Omega\rho^2) L_n^{|m|}(M\Omega\rho^2)^* \\
&= \frac{\mathcal{N}\mathcal{N}^*}{2\,M\,\Omega} \int_0^\infty ds\; \mathrm{e}^{-s}\; s^{|m|}\; L_{n'}^{|m|}(s)\; L_n^{|m|}(s)^* \\
&= \frac{\mathcal{N}\mathcal{N}^*}{2\,M\,\Omega} \frac{(|m|+n)!}{n!}\, \delta_{n,n'}. \qquad \text{(B.24)}
\end{aligned}
$$

Thus the properly normalized wavefunctions $\Psi_{n,m}(\rho,\phi) = f_{n,m}(\rho)\chi_m(\phi)$ are given by

$$
\begin{aligned}
f_{n,m}(\rho) &= \sqrt{2\,M\,\Omega} \sqrt{\frac{n!}{(n+|m|)!}}\, \mathrm{e}^{-M\,\Omega\,\rho^2/2} \left(\sqrt{M\,\Omega}\,\rho\right)^{|m|} L_n^{|m|}(M\,\Omega\,\rho^2), \qquad \text{(B.25)} \\
\chi_m(\phi) &= \frac{1}{\sqrt{2\pi}}\, \mathrm{e}^{i\,m\,\phi}. \qquad \text{(B.26)}
\end{aligned}
$$

Momentum space

Notice the symmmetry of the harmonic oscillator wave equation

$$
\left[\frac{p_x^2+p_y^2}{M\,\Omega} + (M\,\Omega)\,(x^2+y^2)\right]\Psi = \frac{2\,E}{\Omega}\,\Psi, \qquad \text{(B.27)}
$$

under the transformation $p/\sqrt{M\Omega} \longleftrightarrow x\sqrt{M\Omega}$. Thus the solution of the 2-d harmonic oscillator in momentum space can be written as $\tilde{\Psi}_{n,m}(q,\theta) = \tilde{f}_{n,m}(q)\chi_m(\theta)$ with q the conjugate of ρ, θ the conjugate of ϕ (i.e. angle in momentum space), and

$$
\tilde{f}_{n,m}(q) = \tilde{\mathcal{N}}\, \mathrm{e}^{-q^2/(2\,M\,\Omega)} \left(\frac{q}{\sqrt{M\,\Omega}}\right)^{|m|} L_n^{|m|}(q^2/(M\,\Omega)). \qquad \text{(B.28)}
$$

The normalization of the momentum-space wavefunction is fixed by an orthonormality condition similar to Eqn. (B.20). But in momentum space there is an extra factor $1/(2\pi)^2$ for the integration measure

$$
\langle nm|n'm'\rangle = \int \frac{d^2p}{(2\pi)^2}\, \tilde{\Psi}_{nm}(p)^*\, \tilde{\Psi}_{n'm'}(p) = \delta_{nn'}\,\delta_{mm'}. \qquad \text{(B.29)}
$$

Using the same angular wavefunction

$$
\chi_m(\theta) = \frac{1}{\sqrt{2\pi}}\, \mathrm{e}^{i\,m\,\theta} \qquad \text{(B.30)}
$$

as in coordinate space, the normalization factor $\tilde{\mathcal{N}}$ follows from

$$
\int_0^\infty \frac{q\,dq}{(2\pi)^2}\; \tilde{f}_{n,m}(q)^*\; \tilde{f}_{n',m}(q)
$$

$$
\begin{aligned}
&= \int_0^\infty \frac{q\,dq}{(2\pi)^2}\,\tilde{\mathcal{N}}\tilde{\mathcal{N}}^*\,\mathrm{e}^{-q^2/(M\,\Omega)}\,\left(\frac{q^2}{M\,\Omega}\right)^{|m|}\,L_{n'}^{|m|}(q^2/(M\,\Omega))\,L_n^{|m|}(q^2/(M\,\Omega))^* \\
&= \tilde{\mathcal{N}}\tilde{\mathcal{N}}^*\,\frac{M\,\Omega}{2\,(2\pi)^2}\,\int_0^\infty ds\,\mathrm{e}^{-s}\,s^{|m|}\,L_{n'}^{|m|}(s)\,L_n^{|m|}(s)^* \\
&= \tilde{\mathcal{N}}\tilde{\mathcal{N}}^*\,\frac{M\,\Omega}{2\,(2\pi)^2}\,\frac{(|m|+n)!}{n!}\,\delta_{n,n'}. \qquad \text{(B.31)}
\end{aligned}
$$

Thus the properly normalized radial wavefunction in momentum space is

$$
\tilde{f}_{n,m}(q) \;=\; 2\pi\,\sqrt{\frac{2}{M\,\Omega}}\,\sqrt{\frac{n!}{(|m|+n)!}}\,\mathrm{e}^{-q^2/(2\,M\,\Omega)}\,\left(\frac{q}{\sqrt{M\,\Omega}}\right)^{|m|}\,L_n^{|m|}(q^2/(M\,\Omega)) \qquad \text{(B.32)}
$$

With the coordinate-space wavefunction given by Eqs. (B.25) and (B.26), we have

$$
\begin{aligned}
&\tilde{\Psi}_{n,m}(q,\theta) \\
&= \sqrt{\frac{2\,M\,\Omega}{2\pi}}\sqrt{\frac{n!}{(n+|m|)!}}\int d^2x\mathrm{e}^{i\,\vec{p}\cdot\vec{x}}\mathrm{e}^{-M\Omega\rho^2/2}\left(\sqrt{M\Omega}\rho\right)^{|m|}\,L_n^{|m|}(M\Omega\rho^2)\mathrm{e}^{im\phi}. \qquad \text{(B.33)}
\end{aligned}
$$

BIBLIOGRAPHY

[1] D. J. Gross and F. Wilczek, *Phys. Rev. Lett* **30**, 1343 (1973).

[2] H. D. Polotzer, *Phys. Rev. Lett* **30**, 1346 (1973).

[3] J. C. Collins, D. E. Soper and G. Sterman, *Adv. Ser. Direct. High Energy Phys.* **5**, 1(1988) [arXiv:hep-ph/0409313].

[4] M. Gell-Mann, *Phys. Lett.* **8**, 214 (1964).

[5] G. Zweig, *CERN Report No.8181/Th 8419* (1964), *CERN Report No.8419/Th 8412* (1964).

[6] C. N. Yang and R. L. Mills, *Phys. Rev.* **96**, 191 (1954).

[7] H. Fritzsch, M. Gell-Mann and H. Leutwyler, *Phys. Lett.* **B 47**, 365 (1973).

[8] W. A. Caswell, *Phys. Rev. Lett* **33**, 244 (1974).

[9] O. V. Tarasov, A. A. Vladimirov and A. Yu. Zharkov, *Phys. Lett* **B 93**, 429 (1980); S. A. Larin and J. A. M. Vermaseren, *Phys. Lett* **B 303**, 334 (1993).

[10] C. Amsler et al. [Particle Data Group], *Phys. Lett.* **B 667**, 1 (2008).

[11] M. E. Peskin, D. V. Schroeder, *An introduction to Quantum Field Theory.*

[12] P.A.M.Dirac, *Rev. Mod. Phys.* **21**, 392 (1949).

[13] Richard Lloyd, *PhD thesis at ISU*2004.

[14] Richard J. Lloyd and James P. Vary, *Phys. Rev. D* **70**, 014009 (2004) [arXiv:hep-ph/0311179].

[15] H. C. Pauli and S. J. Brodsky, *Phys. Rev. D* **32**, (1985)1993; S. J. Brodsky, H. C. Pauli and S. S. Pinsky, *Quantum Chromodynamics and Other Field Theories on the Light Cone*, *Phys. Reports* **301** (1998) 299 [arXiv:hep-ph/9705477].

[16] M. Burkardt and S. Dalley, *Prog. Part. Nucl. Phys.* **48**, 317 (2002) [arXiv:hep-ph/0112007].

[17] D. Chakrabarti, A. Harindranath and J. P. Vary, *Phys. Rev. D* **69** , (2004) 034502 [arXiv:hep-ph/0309317].

[18] D. Grunewald, E. M. Ilgenfritz, E. V. Prokhvatilov and H. J. Pirner, *Phys. Rev. D* **77** (2008) 014512.

[19] P. Navrátil, J. P. Vary and B. R. Barrett, *Phys. Rev. Lett.* **84** (2000) 5728; *Phys. Rev. C* **62** (2000) 054311.

[20] P. Maris, J. P. Vary and A. M. Shirokov, *Phys. Rev. C* **79** (2009) 014308, [arXiv:nucl-th/0808.3420].

[21] K. G. Wilson, *Nucl. Phys. Proc. Suppl.* **17**, 82 (1990).

[22] J. P. Vary, H. Honkanen, Jun Li, P. Maris, S. J. Brodsky, P. Sternberg, E. G. Ng, and C. Yang, *Proceedings of Science LC2008* 040 (2008) [arXiv:nucl-th/0812.1819].

[23] J. P. Vary, H. Honkanen, Jun Li, P. Maris, S. J. Brodsky, A. Harindranath, G. F. De Teramond, P. Sternberg, E. G. Ng, and C. Yang, [arXiv:nucl-th/0812.1819].

[24] P. Navrátil, V. G. Gueorguiev, J. P. Vary, W. E. Ormand and A. Nogga, *Phys. Rev. Lett.* **99** (2007)042501 [arXiv:nucl-th/0701038].

[25] S. K. Bogner, R. J. Furnstahl, P. Maris, R. J. Perry, A. Schwenk and J. P. Vary, *Nucl. Phys. A* **801**, (2008) 21[arXiv:nucl-th/0708.3754].

[26] P. Sternberg, E. G. Ng, C. Yang, P. Maris, J. P. Vary, M. Sosonkina and H. V. Le, in Proceedings of the 2008 ACM/IEEE Conference on Supercomputing (Austin, Texas,

November 15 - 21, 2008). Conference on High Performance Networking and Computing. IEEE Press, Piscataway, NJ, 1-12. DOI= http://doi.acm.org/10.1145/1413370.1413386.

[27] A. M. Shirokov, J. P. Vary, A. I. Mazur and T. A. Weber, *Phys. Letts. B* **644** (2007) 33 [arXiv:nucl-th/0512105].

[28] A. Karch, E. Katz, D. T. Son and M. A. Stephanov, Phys. Rev. D **74**, 015005 (2006) [arXiv:hep-ph/0602229].

[29] J. Erlich, E. Katz, D. T. Son and M. A. Stephanov, Phys. Rev. Lett. **95**, 261602 (2005) [arXiv:hep-ph/0501128].

[30] G. F. de Teramond and S. J. Brodsky, Phys. Rev. Lett. **102**, 081601 (2009) [arXiv:0809.4899 [hep-ph]].

[31] S. J. Brodsky and G. F. de Teramond, Phys. Lett. B **582**, 211 (2004) [arXiv:hep-th/0310227].

[32] J. Polchinski and M. J. Strassler, Phys. Rev. Lett. **88**, 031601 (2002) [arXiv:hep-th/0109174].

[33] R. J. Lloyd and J. P. Vary, *Phys. Rev. D* **70** (2004) 014009 [arXiv:hep-ph/0311179].

[34] K. Hornbostel, S. J. Brodsky and H. C. Pauli, Phys. Rev. D **41**, 3814 (1990).

[35] V. A. Karmanov, J.-F. Mathiot and A. V. Smirnov, *Phys. Rev. D* **77** (2008) 085028 [arXiv:hep-th/0801.4507]

[36] S. J. Brodsky, J. R. Hiller and G. McCartor, Phys. Rev. D **58**, 025005 (1998) [arXiv:hep-th/9802120].